

**PERIODIC PERTURBATIONS OF CODIMENSION-TWO
BIFURCATIONS WITH A DOUBLE ZERO EIGENVALUE IN
DYNAMICAL SYSTEMS WITH SYMMETRY**

KAZUYUKI YAGASAKI

ABSTRACT. We study bifurcation behavior in periodic perturbations of two-dimensional symmetric systems exhibiting codimension-two bifurcations with a double eigenvalue when the frequencies of the perturbation terms are small. We transform the periodically perturbed system to a simpler one which is a periodic perturbation of the normal form for codimension-two bifurcations with a double zero eigenvalue and symmetry, and apply the subharmonic and homoclinic Melnikov methods to analyze bifurcations occurring in the system. In particular, we show that there exist transverse homoclinic or heteroclinic orbits, which yield chaotic dynamics, in wide parameter regions. These results can be applied to three or higher-dimensional systems and even to infinite-dimensional systems with the assistance of center manifold reduction and the invariant manifold theory. We illustrate our theory for a pendulum subjected to position and velocity feedback control when the desired position is periodic in time. We also give numerical computations by the computer tool `AUTO` to demonstrate the theoretical results.

1. INTRODUCTION

Codimension-two bifurcations are fundamental and interesting phenomena in dynamical systems and have been studied extensively, since the seminal papers of Arnold [1] and Takens [20]. Such bifurcations can occur not only in finite-dimensional systems but also in infinite-dimensional systems. See, e.g., [8, 11, 16–18, 22] and references therein for mathematical explanations on the theory and applications. Two parameters are needed at least for a codimension-two bifurcation point to be generically contained in the parameter space. Among of them, codimension-two bifurcations occurring when the Jacobian matrices of the vector fields at equilibria have a double zero eigenvalue are especially important and now well understood. In particular, different bifurcation diagrams are obtained, depending on whether the systems are symmetric or not [8, 11, 16]. Vast literature on applications exhibiting this type of bifurcation is also found (see, e.g., Section 20.6A of [22]). Similar codimension-two bifurcations can occur for periodic orbits or diffeomorphisms [5, 18].

Moreover, we notice that infinitely many bifurcation points of this type can exist in the two-dimensional parameter space. Actually, it was shown in [27] that this

Date: February 15, 2023.

2020 Mathematics Subject Classification. 34C23; 37G15; 37G25; 37G40; 34D10; 34E10; 34H05; 70Q05.

Key words and phrases. Bifurcation; codimension-two; periodic perturbation; symmetry; Melnikov method; homoclinic orbit; heteroclinic orbit; periodic orbit.

behavior occurs in the three-dimensional system

$$\begin{aligned} \dot{z}_1 &= z_2, \\ \dot{z}_2 &= -\sin z_1 - \delta_0 z_2 + z_3, \\ \dot{z}_3 &= -\alpha z_3 + \gamma(\theta_d - z_1) - \delta_1 z_2, \end{aligned} \quad z = (z_1, z_2, z_3) \in \mathbb{S}^1 \times \mathbb{R} \times \mathbb{R}, \quad (1.1)$$

where $\alpha, \delta_0 > 0$ and $\delta_1, \gamma, \theta_d$ are constants and $\mathbb{S}^1 = \mathbb{R}/2\pi\mathbb{Z}$. Here the system (1.1) represents a pendulum driven by a servo-motor and subjected to position and velocity feedback control with the desired position and velocity given by $z_1 = \theta_d$ and $z_2 = 0$, where z_1 and z_2 , respectively, represent the position and angular velocity of the pendulum; z_3 the torque servo-motor; α the reciprocal of the time constant of the servo-motor; δ_0 the damping constant of the pendulum resulting from servo-motor friction and other sources; and γ and δ_1 , respectively, the position and velocity gain constants of the feedback control.

In this paper, we study bifurcation behavior in periodic perturbations of two-dimensional symmetric systems exhibiting codimension-two bifurcations with a double zero eigenvalue. Specifically, we consider two-dimensional nonautonomous systems of the form

$$\dot{x} = f(x; \mu) + \varepsilon g(x, \omega t), \quad x \in \mathbb{R}^2, \quad (1.2)$$

where ε is a small parameter such that $0 < \varepsilon \ll 1$, $\omega > 0$ is a constant, and $\mu \in \mathbb{R}^2$ represents a control parameter vector. Here $f : \mathbb{R}^2 \times \mathbb{R}^2 \rightarrow \mathbb{R}^2$ is C^4 and symmetric around $x = 0$, i.e.,

$$f(-x; \mu) = -f(x; \mu), \quad (1.3)$$

which yields

$$f(0; \mu) = 0, \quad (1.4)$$

so that the origin $x = 0$ is an equilibrium when $\varepsilon = 0$. Moreover, the Jacobian matrix of $f(x; \mu)$ at $x = 0$ with $\mu = 0$ is assumed to be the 2×2 Jordan normal form with a double zero eigenvalue,

$$D_x f(0; 0) = \begin{pmatrix} 0 & 1 \\ 0 & 0 \end{pmatrix} =: J. \quad (1.5)$$

In such a situation, bifurcation behavior occurring in (1.2) when $\varepsilon = 0$ has been studied extensively and is well described in several textbooks such as [8, 11, 16, 22].

We also assume that $g : \mathbb{R}^2 \times \mathbb{R} \rightarrow \mathbb{R}^2$ is C^2 , and $g(x, \phi)$ is 2π -periodic in ϕ and has mean zero in ϕ for any $x \in \mathbb{R}^2$, i.e.,

$$\int_0^{2\pi} g(x, \phi) d\phi = 0. \quad (1.6)$$

We are interested in the case in which the frequency ω is sufficiently small such that $\omega = O(\varepsilon^{1/4})$. We transform (1.2) to a simpler system which is a periodic perturbation of the normal form for codimension-two bifurcations with a double zero eigenvalue and symmetry, and apply the subharmonic and homoclinic Melnikov methods [16, 22, 24] to analyze bifurcations occurring in (1.2). About the subharmonic Melnikov method, we use the version of [24], which was further sophisticated from the classical theory of [16] and especially enables us to easily determine the stability of detected subharmonic orbits. The reader should consult [24] for its details if he or she is not familiar with this version of the theory. Among the theoretical results presented here, we show that there exist transverse homoclinic or heteroclinic orbits to periodic orbits, which yield chaotic dynamics, in wide parameter regions.

Moreover, we show that many subharmonic orbits can be born at saddle-node bifurcations due to the periodic perturbations. We remark that when $\omega = O(1)$, such codimension-two bifurcations without symmetry, called the Bogdanov-Takens bifurcations, were studied in [28] and transverse homoclinic orbits were proven to exist only in exponentially small parameter regions.

These results can be applied to three or higher-dimensional systems and even to infinite-dimensional systems with the assistance of center manifold reduction [8, 16–18, 22] and the invariant manifold theory [3, 4, 13–15, 21]. We illustrate our theory for the three-dimensional system (1.1) with the desired position given by

$$\theta_d = \varepsilon\beta \cos \omega t + \theta_0, \quad \theta_0 = 0 \text{ or } \pi, \quad (1.7)$$

where $\beta > 0$ is a constant. Here the reader may think that the third equation of (1.2) should also be changed to

$$\dot{z}_3 = -\alpha z_3 + \gamma(\theta_d - z_1) + \delta_1(\dot{\theta}_d - z_2),$$

but its right hand side is rewritten as

$$-\alpha z_3 + \gamma(\varepsilon\tilde{\beta} \cos(\omega t + \tilde{\phi}) + \theta_0 - z_1) - \delta_1 z_2,$$

where

$$\tilde{\beta} = \sqrt{\beta^2 + \omega^2 \beta^2}, \quad \tilde{\phi} = \arctan \omega,$$

so that we only obtain the same equation with different value of β after the time shift $t \rightarrow t + \tilde{\phi}/\omega$. In addition, we give numerical computations by the computer tool AUTO [12] to demonstrate the theoretical results. Periodic and chaotic motions in a similar system with a negligibly small time constant of the servo motor, i.e., $\alpha, \gamma, \delta_1 \gg 1$, were studied by using the subharmonic and homoclinic Melnikov methods as well as the averaging method [19, 25] in [23, 26].

The rest of this paper is organized as follows: In Section 2, we transform (1.2) to the simpler system

$$\dot{y}_1 = y_2, \quad \dot{y}_2 = \nu_1 y_1 + \nu_2 y_2 + s_1 y_1^3 + s_2 y_1^2 y_2 + \varepsilon h(\bar{\omega} t), \quad (1.8)$$

where ν_1, ν_2 represent new control parameters instead of μ , $h(\phi)$ is 2π -periodic and the higher-order terms are ignored. See (2.6) and (2.7) in Section 2 for definitions of $\nu_1, \nu_2, \bar{\omega}, s_j, j = 1, 2$, and $h(\phi)$. In particular, $s_j = 1$ or $-1, j = 1, 2$. Using the subharmonic and homoclinic Melnikov methods, we analyze bifurcations occurring in (1.8) for $s_1 = 1$ and $s_1 = -1$ in Sections 3 and 4, respectively. We discuss three or higher-dimensional symmetric systems in which the linear parts have a double zero eigenvalue, and describe a treatment to apply our theory with assistance of center manifold reduction and the invariant manifold theory in Section 5. Finally, we apply our theory to the example (1.1) with (1.7) and give numerical results to demonstrate the validity of the theoretical ones in Section 6.

2. PERIODIC PERTURBATION OF THE NORMAL FORM

In this section we show that the system (1.2) is transformed into the periodic perturbation (1.8) of the normal form when higher-order terms are ignored. We carry out a transformation used to obtain the normal form of codimension-two bifurcations with a double zero eigenvalue and symmetry for the autonomous part.

Let x_j and μ_j be the j th elements of x and μ , respectively, for $j = 1, 2$ and let

$$a_{jkl} = \frac{\partial^3 f_j}{\partial x_1^k \partial x_2^l}(0; 0), \quad l = 3 - k, \quad k = 0, 1, 2, 3,$$

$$b_{jkl} = \frac{\partial^2 f_j}{\partial x_k \partial \mu_l}(0; 0), \quad k, l = 1, 2,$$

so that

$$f(x; \mu) = Jx + \begin{pmatrix} \frac{1}{6}a_{130}x_1^3 + \frac{1}{2}a_{121}x_1^2x_2 + \frac{1}{2}a_{112}x_1x_2^2 + \frac{1}{6}a_{103}x_2^3 \\ \frac{1}{6}a_{230}x_1^3 + \frac{1}{2}a_{221}x_1^2x_2 + \frac{1}{2}a_{212}x_1x_2^2 + \frac{1}{6}a_{203}x_2^3 \end{pmatrix} \\ + \begin{pmatrix} (b_{111}\mu_1 + b_{112}\mu_2)x_1 + (b_{121}\mu_1 + b_{122}\mu_2)x_2 \\ (b_{211}\mu_1 + b_{212}\mu_2)x_1 + (b_{221}\mu_1 + b_{222}\mu_2)x_2 \end{pmatrix} + \text{h.o.t.}, \quad (2.1)$$

where ‘h.o.t.’ represents higher-order terms than $O(|x|^3)$ and $O(|\mu||x|)$. Note that by (1.3) and (1.4) no constant and even-order terms with respect to x appear in (2.1). Assume that

$$c := \frac{1}{6}a_{230} \neq 0, \quad d := \frac{1}{2}(a_{221} + a_{130}) \neq 0. \quad (2.2)$$

Using the transformation

$$x = \xi + \begin{pmatrix} (\frac{1}{6}a_{121} + \frac{1}{12}a_{212})\xi_1^3 + (\frac{1}{4}a_{112} + \frac{1}{12}a_{203})\xi_1^2\xi_2 \\ -\frac{1}{6}a_{130}\xi_1^3 + \frac{1}{4}a_{212}\xi_1^2\xi_2 + \frac{1}{6}a_{203}\xi_1\xi_2^2 - \frac{1}{6}a_{103}\xi_2^3 \end{pmatrix}, \quad \xi = (\xi_1, \xi_2) \in \mathbb{R}^2,$$

in (1.2), we have

$$\dot{\xi} = J\xi + \begin{pmatrix} 0 \\ c\xi_1^3 + d\xi_1^2\xi_2 \end{pmatrix} \\ + \begin{pmatrix} (b_{111}\mu_1 + b_{112}\mu_2)\xi_1 + (b_{121}\mu_1 + b_{122}\mu_2)\xi_2 \\ (b_{211}\mu_1 + b_{212}\mu_2)\xi_1 + (b_{221}\mu_1 + b_{222}\mu_2)\xi_2 \end{pmatrix} + \varepsilon g_0(\omega t) + \text{h.o.t.}, \quad (2.3)$$

where ‘h.o.t.’ represents higher-order terms than $O(|\xi|^3)$, $O(|\mu||\xi|)$ and $O(\varepsilon)$, and $g_0(\phi) = g(0, \phi)$. Moreover, we carry out the transformation

$$\xi = \eta - \begin{pmatrix} 0 \\ (b_{111}\mu_1 + b_{112}\mu_2)\eta_1 + (b_{121}\mu_1 + b_{122}\mu_2)\eta_2 \end{pmatrix}, \quad \eta = (\eta_1, \eta_2) \in \mathbb{R}^2,$$

in (2.3) to obtain

$$\dot{\eta}_1 = \eta_2 + \varepsilon g_{01}(\omega t) + \text{h.o.t.},$$

$$\dot{\eta}_2 = \tilde{\mu}_1\eta_1 + \tilde{\mu}_2\eta_2 + c\eta_1^3 + d\eta_1^2\eta_2 + \varepsilon g_{02}(\omega t) + \text{h.o.t.}, \quad (2.4)$$

where $g_{0j}(\phi)$ is the j th component of $g_0(\phi)$ and

$$\tilde{\mu}_1 = b_{211}\mu_1 + b_{212}\mu_2, \quad \tilde{\mu}_2 = (b_{111} + b_{221})\mu_1 + (b_{112} + b_{222})\mu_2.$$

Finally, changing the time variable as $t \rightarrow |c/d|t$ and letting

$$y_1 = \frac{|d|}{\sqrt{|c|}}\eta_1, \quad y_2 = \frac{|d|^2}{|c|^{3/2}}(\eta_2 + \varepsilon g_{01}(\omega t)) + \text{h.o.t.} \quad (2.5)$$

in (2.4), we obtain

$$\dot{y}_1 = y_2, \quad \dot{y}_2 = \nu_1 y_1 + \nu_2 y_2 + s_1 y_1^3 + s_2 y_1^2 y_2 + \varepsilon h(\bar{\omega} t) + \text{h.o.t.},$$

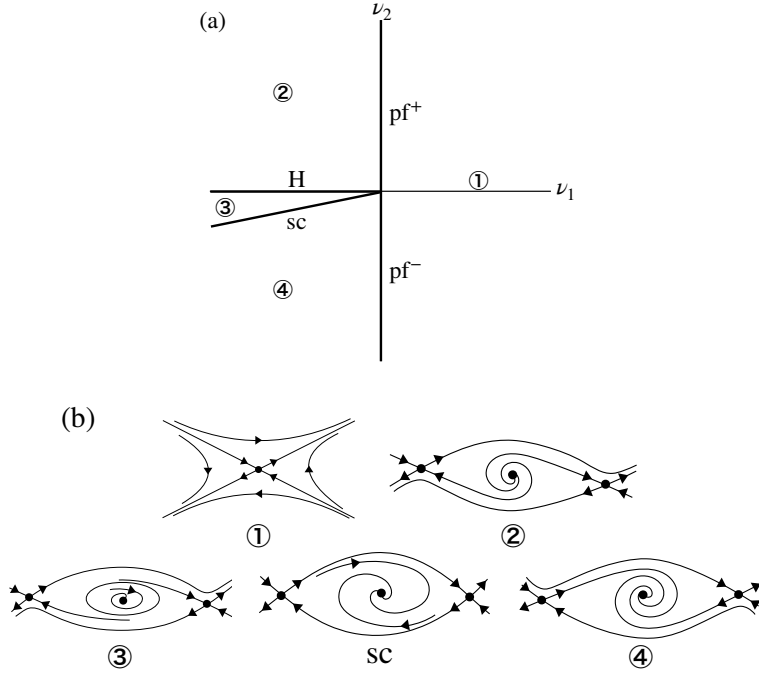


FIGURE 1. Bifurcations of (1.8) with $s_1 = s_2 = 1$ for $\varepsilon = 0$: (a) Bifurcation sets; (b) Phase portraits. pf^\pm , H and sc represent pitchfork, Hopf and heteroclinic bifurcations, respectively.

where

$$\begin{aligned} \nu_1 &= \left| \frac{d}{c} \right|^2 \tilde{\mu}_1 = \left| \frac{d}{c} \right|^2 (b_{211}\mu_1 + b_{212}\mu_2), \\ \nu_2 &= \left| \frac{d}{c} \right| \tilde{\mu}_2 = \left| \frac{d}{c} \right| ((b_{111} + b_{221})\mu_1 + (b_{112} + b_{222})\mu_2), \\ s_1 &= \text{sign } c, \quad s_2 = \text{sign } d, \quad \bar{\omega} = \left| \frac{d}{c} \right| \omega \end{aligned} \tag{2.6}$$

and

$$h(\phi) = \frac{|d|^3}{|c|^{5/2}} g_{02}(\phi). \tag{2.7}$$

Here we have assumed that $\omega = o(1)$. We obtain the following proposition.

Proposition 2.1. *Assume that (2.2) holds. Then the system (1.2) is transformed into (1.8) when the higher-order terms are ignored. Moreover,*

$$\int_0^{2\pi} h(\phi) d\phi = 0. \tag{2.8}$$

Proof. It remains to prove (2.8) but it is obvious from (1.6). \square

We display bifurcation sets and phase portraits of (1.8) with $\varepsilon = 0$ and $s_1 = 1$ (resp. $s_1 = -1$) for $s_2 = 1$ and -1 , respectively, in Figs. 1 and 2 (resp. in Figs. 3 and 4). For $s_1 = 1$, when $s_2 = 1$ (resp. $s_2 = -1$), (i) a pitchfork bifurcation occurs

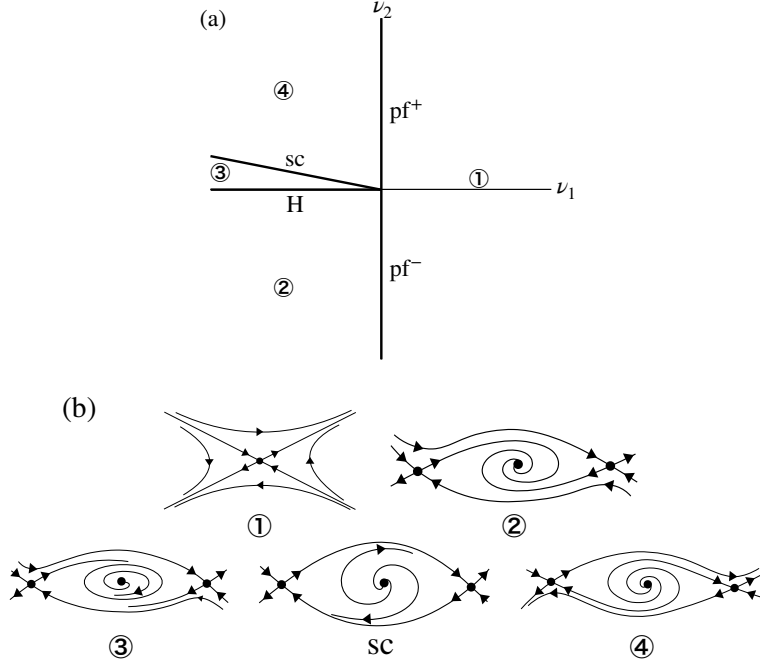


FIGURE 2. Bifurcations of (1.8) with $s_1 = 1$ and $s_2 = -1$ for $\varepsilon = 0$: (a) Bifurcation sets; (b) Phase portraits. See the caption of Fig. 1 for the meaning of the symbols.

on $\nu_1 = 0$ and $\nu_2 \neq 0$; (ii) a Hopf bifurcation occurs on $\nu_2 = 0$ and $\nu_1 < 0$; (iii) a (double) heteroclinic bifurcation (saddle connection) occurs near $\nu_2 = \nu_1/5 < 0$ (resp. near $\nu_2 = -\nu_1/5 > 0$). In region ① there is a saddle; in region ② there are one source (resp. sink) and two saddles; in region ③ there are one sink (resp. source), two saddles and one unstable (resp. stable) periodic orbit; in region ④ there are one sink (resp. source) and two saddles. On the curve *sc*, there are a pair of heteroclinic orbits.

On the other hand, for $s_1 = -1$, when $s_2 = 1$ (resp. $s_2 = -1$), (i) a pitchfork bifurcation occurs on $\nu_1 = 0$ and $\nu_2 \neq 0$; (ii) a Hopf bifurcation occurs on $\nu_2 = 0$ and $\nu_1 < 0$; (iii) a (double) Hopf bifurcation occurs at $\nu_2 = -\nu_1 < 0$ (resp. $\nu_2 = \nu_1 > 0$); (iv) a (double) homoclinic bifurcation occurs near $\nu_2 = -4\nu_1/5 < 0$ (resp. near $\nu_2 = 4\nu_1/5 > 0$); (v) a saddle-node bifurcation of periodic orbits occurs near $\nu_2 = -c\nu_1 < 0$ (resp. near $\nu_2 = c\nu_1 > 0$) with $c \approx 0.752$. In region ① there is a source (resp. sink); in region ② there are a sink (resp. source) and unstable (resp. stable) periodic orbit; in region ③ there are one saddle, two sinks (resp. sources) and one unstable (resp. stable) periodic orbit; in region ④ there are one saddle, two sources (resp. sinks), and one stable and unstable periodic orbits; in region ⑤ there are one saddle, two sources (resp. sinks) and one unstable (resp. stable) periodic orbit; in region ⑥ there are one saddle and two sources (resp. sinks). On the curve *sc*, there are a pair of homoclinic orbits. See [8, 16] for more details.

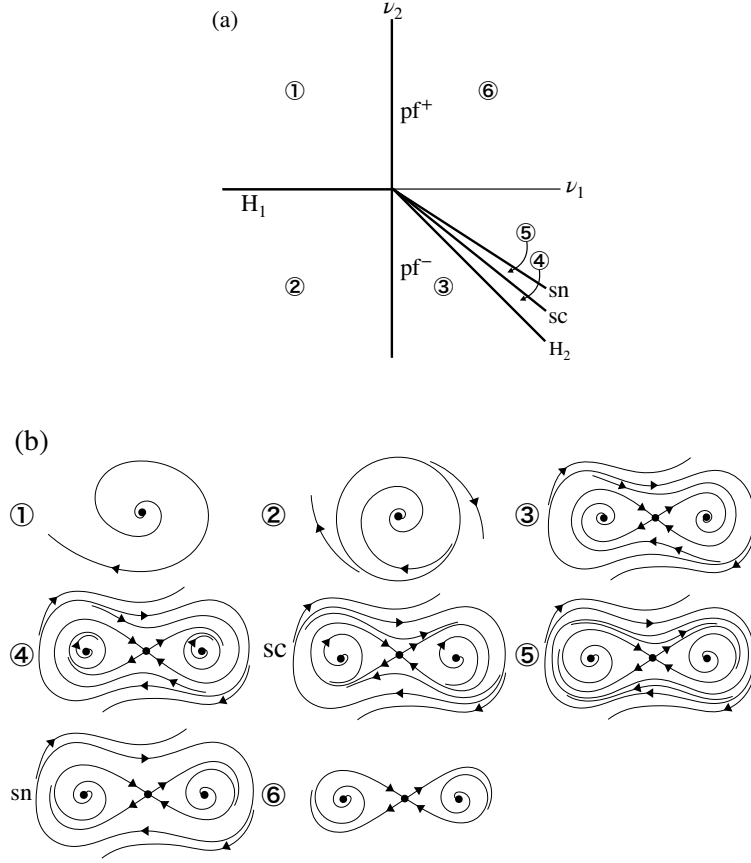


FIGURE 3. Bifurcations of (1.8) with $s_1 = -1$ and $s_2 = 1$ for $\varepsilon = 0$: (a) Bifurcation sets; (b) Phase portraits. pf^\pm , H_j , $j = 1, 2$, and sc represent pitchfork, Hopf and homoclinic bifurcations, respectively, while sn represents saddle-node bifurcations of periodic orbits.

3. MELNIKOV ANALYSES FOR $s_1 = 1$

In this and the next sections, using the subharmonic and homoclinic Melnikov methods [16, 22, 24], we analyze the periodically perturbed system (1.8) to describe bifurcations occurring in (1.2) near $(x, \mu) = (0, 0)$. We begin with the case of $s_1 = 1$.

3.1. Preliminaries. Assume that $|\nu_1|, |\nu_2| \ll 1$, $\nu_1 < 0$, $\nu_2 = O(\nu_1)$ and $\varepsilon = O(\nu_1^2)$. Let $\hat{\varepsilon}$ be a small positive parameter such that $\nu_1 = -\hat{\varepsilon}^2$, and introduce the new state variables $\zeta = (\zeta_1, \zeta_2)$ and the new parameter $\hat{\nu} = O(1)$ as

$$y_1 = \sqrt{-\nu_1}\zeta_1, \quad y_2 = -\nu_1\zeta_2, \quad \hat{\nu} = -\nu_2/\nu_1. \quad (3.1)$$

Rescaling the time variable t as $t \rightarrow \sqrt{-\nu_1}t$, we rewrite (1.8) as

$$\dot{\zeta}_1 = \zeta_2, \quad \dot{\zeta}_2 = -\zeta_1 + \zeta_1^3 + \hat{\varepsilon}(\hat{\nu}\zeta_2 + s_2\zeta_1^2\zeta_2 + \Delta h(\hat{\omega}t)), \quad (3.2)$$

where

$$\hat{\omega} = \frac{\bar{\omega}}{\hat{\varepsilon}} = \left| \frac{d}{c} \right| \frac{\omega}{\hat{\varepsilon}} = O(1), \quad \Delta = \frac{\varepsilon}{\hat{\varepsilon}^4} = O(1). \quad (3.3)$$

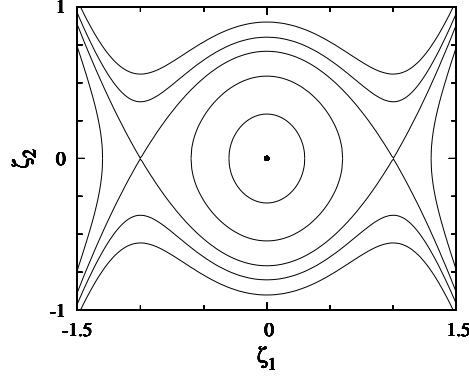


FIGURE 5. Phase portraits of (3.4).

Moreover, inside the pair of heteroclinic orbits, there exists a one-parameter family of periodic orbits,

$$\zeta^k(t) = \left(\begin{array}{c} \frac{\sqrt{2}k}{\sqrt{k^2+1}} \operatorname{sn} \left(\frac{t}{\sqrt{k^2+1}} \right), \\ \frac{\sqrt{2}k}{k^2+1} \operatorname{cn} \left(\frac{t}{\sqrt{k^2+1}} \right) \operatorname{dn} \left(\frac{t}{\sqrt{k^2+1}} \right) \end{array} \right), \quad k \in (0, 1), \quad (3.6)$$

where $\operatorname{sn}, \operatorname{cn}, \operatorname{dn}$ represent Jacobi's elliptic functions with elliptic modulus k . The period of $\zeta^k(t)$ is given by

$$T^k = 4K(k)\sqrt{k^2+1},$$

where $K(k)$ is the complete elliptic integral of the first kind,

$$K(k) = \int_0^{\pi/2} \frac{d\psi}{\sqrt{1-k^2 \sin^2 \psi}}.$$

See [7] for necessary information on elliptic functions and complete elliptic integrals. The phase portrait of (3.4) is displayed in Fig. 5.

3.2. Heteroclinic orbits. We apply the homoclinic Melnikov methods [16, 22]. For $\hat{\varepsilon} > 0$ sufficiently small we easily see that the system (3.2) has hyperbolic periodic orbits, of which the stable and unstable manifolds may intersect, near $\zeta = (\pm 1, 0)$. See [16, 22]. We compute the Melnikov functions for $\zeta_{\pm}^h(t)$ as

$$\begin{aligned} M_{\pm}(\phi; \hat{\nu}) &= \int_{-\infty}^{\infty} \zeta_{2\pm}^h(t) [\hat{\nu} \zeta_{2\pm}^h(t) + s_2 \zeta_{1\pm}^h(t)^2 \zeta_{2\pm}^h(t) + \Delta h(\hat{\omega}t + \phi)] dt \\ &= \frac{4}{3\sqrt{2}} \hat{\nu} + \frac{2\sqrt{2}}{15} s_2 \pm \Delta \hat{h}(\phi), \end{aligned}$$

where

$$\hat{h}(\phi) = \int_{-\infty}^{\infty} \zeta_{2+}^h(t) h(\hat{\omega}t + \phi) dt. \quad (3.7)$$

We have the following property for the function $\hat{h}(\phi)$.

Lemma 3.1. *If $h(\phi) \not\equiv 0$, then*

$$\hat{h}_{\max} = \max_{\phi \in \mathbb{S}^1} \hat{h}(\phi) > 0 \quad \text{and} \quad \hat{h}_{\min} = \min_{\phi \in \mathbb{S}^1} \hat{h}(\phi) < 0, \quad (3.8)$$

where \mathbb{S}^1 is the circle of length 2π .

Proof. Noting that it is C^2 , we expand $h(\phi)$ in a Fourier series as

$$h(\phi) = \sum_{j=-\infty}^{\infty} h_j e^{ij\phi}, \quad h_j = \frac{1}{2\pi} \int_0^{2\pi} h(\phi) e^{-ij\phi} d\phi,$$

so that

$$\hat{h}(\phi) = \sum_{j=-\infty}^{\infty} h_j \tilde{\zeta}_{2+}(j\hat{\omega}) e^{ij\phi},$$

where

$$\tilde{\zeta}_{2+}(\chi) = \int_{-\infty}^{\infty} \zeta_{2+}^h(t) e^{i\chi t} dt = \begin{cases} \sqrt{2\pi}\chi \operatorname{csch}(\sqrt{2\pi}\chi/2) & \text{for } \chi \neq 0; \\ 2 & \text{for } \chi = 0, \end{cases} \quad (3.9)$$

which is not zero for any $\chi \in \mathbb{R}$. Here we have used the fact that the integral in (3.9) is uniformly convergent in $j \in \mathbb{Z}$. Hence, if $h(\phi) \not\equiv 0$, then $\hat{h}_j \neq 0$ for some $j \in \mathbb{Z}$ at least and consequently $\hat{h}(\phi) \not\equiv 0$.

On the other hand, we easily see that the integral in (3.7) is uniformly convergent in ϕ since the integrand exponentially tends to 0. Hence,

$$\begin{aligned} \int_0^{2\pi} \hat{h}(\phi) d\phi &= \int_0^{2\pi} \left[\int_{-\infty}^{\infty} \zeta_{2\pm}^h(t) h(\hat{\omega}t + \phi) dt \right] d\phi \\ &= \int_{-\infty}^{\infty} \zeta_{2\pm}^h(t) \left[\int_0^{2\pi} h(\hat{\omega}t + \phi) d\phi \right] dt = 0, \end{aligned}$$

which yields (3.8). \square

Assume that $h(\phi) \not\equiv 0$. If

$$-\Delta \hat{h}_{\max} < \frac{4}{3\sqrt{2}} \hat{\nu} + \frac{2\sqrt{2}}{15} s_2 < -\Delta \hat{h}_{\min} \quad \text{and} \quad \Delta \hat{h}_{\min} < \frac{4}{3\sqrt{2}} \hat{\nu} + \frac{2\sqrt{2}}{15} s_2 < \Delta \hat{h}_{\max}$$

i.e.,

$$\left(\frac{3\sqrt{2}}{4} \Delta \hat{h}_{\max} + \frac{1}{5} s_2 \right) \nu_1 < \nu_2 < \left(\frac{3\sqrt{2}}{4} \Delta \hat{h}_{\min} + \frac{1}{5} s_2 \right) \nu_1, \quad \nu_1 < 0, \quad (3.10)$$

and

$$\left(-\frac{3\sqrt{2}}{4} \Delta \hat{h}_{\min} + \frac{1}{5} s_2 \right) \nu_1 < \nu_2 < \left(-\frac{3\sqrt{2}}{4} \Delta \hat{h}_{\max} + \frac{1}{5} s_2 \right) \nu_1, \quad \nu_1 < 0, \quad (3.11)$$

then the Melnikov functions $M_{\pm}(\phi; \hat{\nu})$ cross the zero topologically. Using arguments given in [16, 22], we obtain the following result.

Theorem 3.2. *Suppose that $h(\phi) \not\equiv 0$. If condition (3.10) (resp. (3.11)) holds for $|\nu_1|, |\nu_2|, \varepsilon > 0$ sufficiently small, then the left branch of the stable manifold (resp. of the unstable manifold) of a periodic orbit near $\zeta = (1, 0)$ intersect the right branch of the unstable manifold (resp. of the stable manifold) of a periodic orbit*

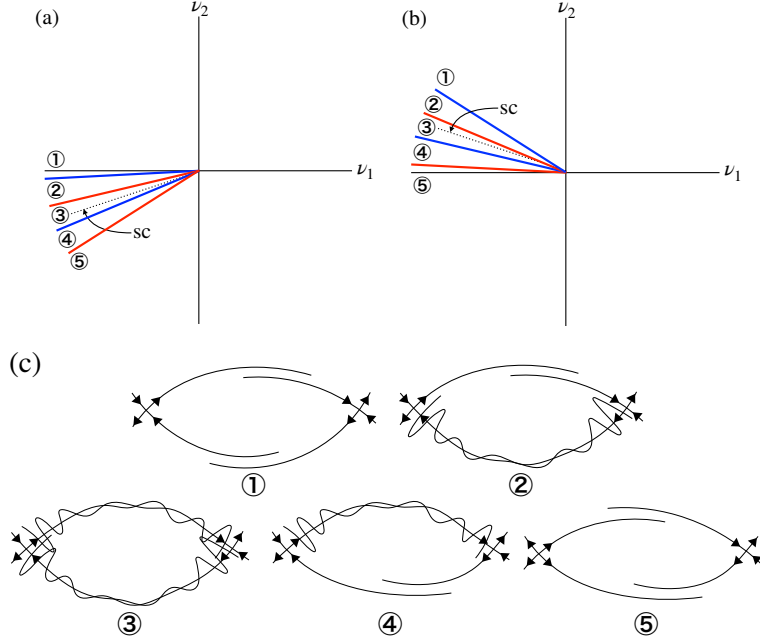


FIGURE 6. Heteroclinic bifurcations in (3.2): (a) Approximate bifurcation sets for $s_2 = 1$; (b) for $s_2 = -1$; (c) stable and unstable manifolds for a Poincaré map.

near $\zeta = (-1, 0)$ topologically transversely in (3.2) and hence in (1.2). Moreover, heteroclinic bifurcations occur near the four curves

$$\nu_2 = \left(\frac{3\sqrt{2}}{4} \Delta \hat{h}_{\max} + \frac{1}{5} s_2 \right) \nu_1, \quad \nu_2 = \left(\frac{3\sqrt{2}}{4} \Delta \hat{h}_{\min} + \frac{1}{5} s_2 \right) \nu_1, \quad \nu_1 < 0, \quad (3.12)$$

$$\nu_2 = \left(-\frac{3\sqrt{2}}{4} \Delta \hat{h}_{\min} + \frac{1}{5} s_2 \right) \nu_1, \quad \nu_2 = \left(-\frac{3\sqrt{2}}{4} \Delta \hat{h}_{\max} + \frac{1}{5} s_2 \right) \nu_1, \quad \nu_1 < 0. \quad (3.13)$$

Remark 3.3. *In the overlap parameter region between (3.10) and (3.11), there exists a heteroclinic cycle and consequently topologically transverse homoclinic orbits to the periodic orbits near $\zeta = (\pm 1, 0)$. See Section 26.1 of [22] for more details on the fact. Such homoclinic orbits also yield chaotic motions in (3.2) and (1.2) like geometrically transverse ones. See [6] for more details.*

Figures 6(a) and (b) show the approximate heteroclinic bifurcation sets detected by Theorem 3.2 for $s_2 = 1$ and -1 , respectively. Here we have assumed that $|\hat{h}_{\min}| < |\hat{h}_{\max}|$. The red and blue lines correspond to the bifurcation sets (3.12) and (3.13), respectively. Figure 6(c) shows the behavior of the stable and unstable manifolds of the periodic orbits near $\zeta = (\pm 1, 0)$ for a Poincaré map whose orbit is given by sampling $(\zeta_1(t), \zeta_2(t))$ at every period, in regions ①-⑤ of both figures. In particular, in region ③, a heteroclinic cycle is constructed and consequently chaotic motions occur, as stated in Remark 3.3. When $|\hat{h}_{\min}| > |\hat{h}_{\max}|$, the loci of

the red and blue lines are exchanged in Figs. 6(a) and (b) and when $|\hat{h}_{\min}| = |\hat{h}_{\max}|$, regions ② and ④ disappear or their widths becomes $o(\sqrt{-\nu_1})$.

3.3. Subharmonic orbits. We next apply the subharmonic Melnikov method [24]. Since Eq. (3.4) is a single-degree-of-freedom Hamiltonian and integrable, there exists a symplectic transformation from ζ to the *action-angle coordinates* (I, ϕ) , e.g., as described in Chapter 10 of [2]. Let $\Omega^k = 2\pi/T^k$ and I^k , respectively, represent the angular frequency and action of $\zeta^k(t)$, where

$$I^k = \frac{1}{2\pi} \int_0^{T^k} \zeta_2^k(t)^2 dt. \quad (3.14)$$

We first compute the derivative $d\Omega^k/dI^k$, which is required in application of the theory. Since the symplectic transformation is explicitly obtained in general, the reader may think that it is difficult, but it is not, as we see below.

The Hamiltonian energy for $\zeta^k(t)$ is given by

$$H^k = \frac{k^2}{(k^2 + 1)^2},$$

so that

$$\frac{dH^k}{dk} = \frac{2k(1 - k^2)}{(k^2 + 1)^3} > 0.$$

Since

$$\frac{dH^k}{dI^k} = \Omega^k = \frac{\pi}{2K(k)\sqrt{k^2 + 1}} > 0$$

and

$$\frac{d}{dk} [(1 - k^2)K(k) - (1 + k^2)E(k)] = -3kE(k) < 0,$$

we have

$$\frac{dI^k}{dk} = \frac{dH^k/dk}{dH^k/dI^k} > 0$$

and

$$\frac{d\Omega^k}{dk} = \frac{\pi}{2k(1 - k^2)(1 + k^2)^{3/2}K(k)^2} [(1 - k^2)K(k) - (1 + k^2)E(k)] < 0,$$

where $E(k)$ is the complete elliptic integral of the second kind,

$$E(k) = \int_0^{\pi/2} \sqrt{1 - k^2 \sin^2 \psi} d\psi.$$

Here we have also used $K(0) = E(0) = \pi/2$ and

$$\frac{dK}{dk}(k) = \frac{1}{k(1 - k^2)} (E(k) - (1 - k^2)K(k)), \quad \frac{dE}{dk}(k) = \frac{1}{k} (E(k) - K(k)).$$

Thus, we obtain

$$\frac{d\Omega^k}{dI^k} = \frac{d\Omega^k/dk}{dI^k/dk} < 0.$$

Let $nT^k = m\hat{T}$ for $m, n > 0$ relatively prime integers, where $\hat{T} = |c/d|\varepsilon T$. We compute the subharmonic Melnikov functions as

$$\begin{aligned} M^{m/n}(\phi; \hat{\nu}) &= \int_0^{m\hat{T}} \zeta_2^k(t) [\hat{\nu}\zeta_2^k(t) + s_2\zeta_1^k(t)^2\zeta_2^k(t) + \Delta h(\hat{\omega}t + \phi)] dt \\ &= \hat{\nu}J_1(k, n) + s_2J_2(k, n) + \Delta\hat{h}^{m/n}(\phi) \end{aligned}$$

and

$$L^{m/n}(\phi; \hat{\nu}) = \int_0^{m\hat{T}} (\hat{\nu} + s_2\zeta_1^k(t)^2) dt = m\hat{\nu}\hat{T} + s_2J_3(k, n),$$

where

$$\begin{aligned} J_1(k, n) &= \int_0^{m\hat{T}} \zeta_2^k(t)^2 dt = \frac{2k^2}{(k^2+1)^2} \int_0^{m\hat{T}} \operatorname{cn}^2\left(\frac{t}{\sqrt{k^2+1}}\right) \operatorname{dn}^2\left(\frac{t}{\sqrt{k^2+1}}\right) dt \\ &= \frac{8n}{3(k^2+1)^{3/2}} [(k^2+1)E(k) - k'^2K(k)] > 0, \end{aligned}$$

$$\begin{aligned} J_2(k, n) &= \int_0^{m\hat{T}} \zeta_1^k(t)^2\zeta_2^k(t)^2 dt \\ &= \frac{4k^4}{(k^2+1)^3} \int_0^{m\hat{T}} \operatorname{sn}^2\left(\frac{t}{\sqrt{k^2+1}}\right) \operatorname{cn}^2\left(\frac{t}{\sqrt{k^2+1}}\right) \operatorname{dn}^2\left(\frac{t}{\sqrt{k^2+1}}\right) dt \\ &= \frac{16n}{15(k^2+1)^{5/2}} [2(k^4 - k^2 + 1)E(k) - k'(2 - k^2)K(k)] > 0, \end{aligned}$$

$$\begin{aligned} J_3(k, n) &= \int_0^{m\hat{T}} \zeta_1^k(t)^2 dt = \frac{2k^2}{k^2+1} \int_0^{m\hat{T}} \operatorname{sn}^2\left(\frac{t}{\sqrt{k^2+1}}\right) dt \\ &= \frac{8n}{\sqrt{k^2+1}} [K(k) - E(k)] > 0 \end{aligned}$$

and

$$\hat{h}^{m/n}(\phi) = \int_0^{m\hat{T}} \zeta_2^k(t)h(\hat{\omega}t + \phi)dt, \quad (3.15)$$

where $k' = \sqrt{1 - k^2}$ is complementary elliptic modulus.

Lemma 3.4. *If $\hat{h}^{m/n}(\phi) \not\equiv 0$, then*

$$\hat{h}_{\max}^{m/n} = \max_{\phi \in \mathbb{S}^1} \hat{h}^{m/n}(\phi) > 0 \quad \text{and} \quad \hat{h}_{\min}^{m/n} = \min_{\phi \in \mathbb{S}^1} \hat{h}^{m/n}(\phi) < 0. \quad (3.16)$$

Proof. We easily see that

$$\begin{aligned} \int_0^{2\pi} \hat{h}^{m/n}(\phi) d\phi &= \int_0^{2\pi} \left[\int_0^{m\hat{T}} \zeta_2^k(t)h(\hat{\omega}t + \phi) dt \right] d\phi \\ &= \int_0^{m\hat{T}} \zeta_2^k(t) \left[\int_0^{2\pi} h(\hat{\omega}t + \phi) d\phi \right] dt = 0. \end{aligned}$$

Thus, if $\hat{h}^{m/n}(\phi) \not\equiv 0$, then Eq. (3.16) holds. \square

Theorem 3.5. *Suppose that $\hat{h}^{m/n}(\phi) \not\equiv 0$ and take ν_1 or ν_2 as a control parameter. Then saddle-node bifurcations of $m\hat{T}$ -periodic (resp. mT -periodic) orbits occur near*

$$\nu_2 = \frac{\Delta \hat{h}_{\max}^{m/n} + s_2 J_2(k, n)}{J_1(k, n)} \nu_1 \quad \text{and} \quad \nu_2 = \frac{\Delta \hat{h}_{\min}^{m/n} + s_2 J_2(k, n)}{J_1(k, n)} \nu_1, \quad \nu_1 < 0 \quad (3.17)$$

in (3.2) (resp. in (1.2)).

Proof. Suppose that the first (resp. second) condition in (3.17) holds, i.e.,

$$\hat{\nu} J_1(k, n) + s_2 J_2(k, n) = -\Delta \hat{h}_{\max}^{m/n} \quad (\text{resp.} \quad -\Delta \hat{h}_{\min}^{m/n}).$$

We assume that $\hat{h}^{m/n}(\phi)$ attains the maximum (resp. minimum) at $\phi = \phi_0$, so that

$$\frac{d\hat{h}^{m/n}}{d\phi}(\phi_0) = 0.$$

If in addition

$$\frac{d^2 \hat{h}^{m/n}}{d\phi^2}(\phi_0) < 0 \quad (\text{resp.} > 0), \quad (3.18)$$

then the subharmonic Melnikov function $M^{m/n}(\phi; \hat{\nu})$ satisfies

- (i) $M^{m/n}(\phi_0; \hat{\nu}) = 0$;
- (ii) $\frac{\partial M^{m/n}}{\partial \phi}(\phi_0; \hat{\nu}) = 0$;
- (iii) $\frac{\partial^2 M^{m/n}}{\partial \phi^2}(\phi_0; \hat{\nu}) \neq 0$;
- (iv) $\frac{\partial M^{m/n}}{\partial \hat{\nu}}(\phi_0; \hat{\nu}) \neq 0$,

which yields the conclusion by Theorem 4.1 of [24]. If condition (3.18) does not hold, then we slightly modify the theorem to obtain the desired result. \square

Remark 3.6. *It follows from Theorem 3.2 of [24] that one of periodic orbits born at the saddle-node bifurcation detected in Theorem 3.5 is of a sink (resp. a source) type and the other is of a saddle type if*

$$L^{m/n}(\phi; \hat{\nu}) = m\hat{\nu} + s_2 J_3(k, n) < 0 \quad (\text{resp.} > 0)$$

i.e.,

$$\nu_2 < \frac{s_2 J_3(k, n)}{m\hat{T}} \nu_1 \quad \left(\text{resp.} \quad \nu_2 > \frac{s_2 J_3(k, n)}{m\hat{T}} \nu_1 \right). \quad (3.19)$$

Hence, the former changes its stability from a source type to a sink one or vice versa near

$$L^{m/n}(\phi; \hat{\nu}) = m\hat{\nu} + s_2 J_3(k, n) = 0, \quad \text{i.e.,} \quad \nu_2 = \frac{s_2 J_3(k, n)}{m\hat{T}} \nu_1, \quad \nu_1 < 0. \quad (3.20)$$

This suggests that a Hopf bifurcation may occur there.

Figures 7(a) and (b), show the approximate saddle-node bifurcation sets detected by Theorem 3.5 for $s_2 = 1$ and -1 , respectively. Figure 7(c) shows the behavior of a Poincaré map near the resonant periodic orbit $\zeta^k(t)$ with $nT^k = m\hat{T}$ for $(m, n) = (3, 1)$ when periodic orbits of sink and saddle types appear, in the region between the two bifurcation curves in both figures.

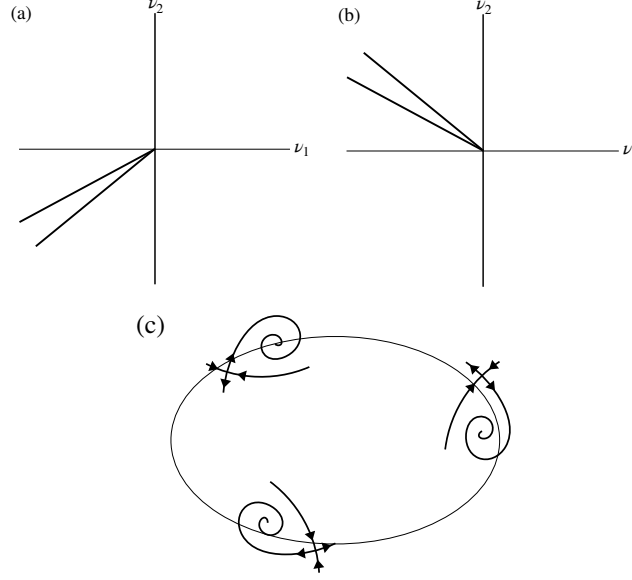


FIGURE 7. Saddle-node bifurcations in (3.2): (a) Approximate bifurcation sets for $s_2 = 1$; (b) for $s_2 = -1$; (c) behavior of a Poincaré map near the unperturbed periodic orbit when periodic orbits of sink and saddle types appear, where $(m, n) = (3, 1)$.

4. MELNIKOV ANALYSES FOR $s_1 = -1$

We turn to the case of $s_1 = -1$ in (1.8). Assume that $|\nu_1|, |\nu_2| \ll 1$, $\nu_2 = O(\nu_1)$ and $\varepsilon = O(\nu_1^2)$. We discuss the two cases of $\nu_1 < 0$ and of $\nu_1 > 0$ separately.

4.1. **Case of $\nu_1 < 0$.** Let $\hat{\varepsilon}$ be a small positive parameter such that $\nu_1 = -\hat{\varepsilon}^2$, and introduce the new state variables $\zeta = (\zeta_1, \zeta_2)$ and the new parameter $\hat{\nu} = O(1)$ as in (3.1). Rescaling the time variable t as $t \rightarrow \sqrt{-\nu_1} t$, we rewrite (1.8) as

$$\dot{\zeta}_1 = \zeta_2, \quad \dot{\zeta}_2 = -\zeta_1 - \zeta_1^3 + \hat{\varepsilon}(\hat{\nu}\zeta_2 + s_2\zeta_1^2\zeta_2 + \Delta h(\hat{\omega}t)), \quad (4.1)$$

where $\nu_1 = -\hat{\varepsilon}^2$, and $\hat{\omega}$ and Δ are given by (3.3).

When $\hat{\varepsilon} = 0$, the system (4.1) becomes

$$\dot{\zeta}_1 = \zeta_2, \quad \dot{\zeta}_2 = -\zeta_1 - \zeta_1^3, \quad (4.2)$$

which is a planar Hamiltonian system with the Hamiltonian

$$H(\zeta) = \frac{1}{2}\zeta_2^2 + \frac{1}{2}\zeta_1^2 + \frac{1}{4}\zeta_1^4.$$

The unperturbed system (4.2) has a one-parameter family of periodic orbits,

$$\zeta^k(t) = \left(\frac{\sqrt{2}k}{\sqrt{1-2k^2}} \operatorname{cn} \left(\frac{t}{\sqrt{1-2k^2}} \right), \right. \\ \left. - \frac{\sqrt{2}k}{1-2k^2} \operatorname{sn} \left(\frac{t}{\sqrt{1-2k^2}} \right) \operatorname{dn} \left(\frac{t}{\sqrt{1-2k^2}} \right) \right), \quad k \in (0, 1/\sqrt{2}), \quad (4.3)$$

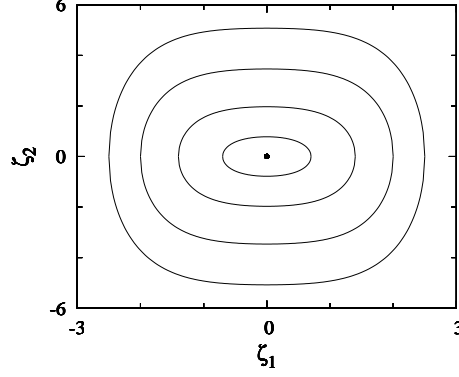


FIGURE 8. Phase portraits of (4.2).

where k represents the elliptic modulus of the Jacobi's elliptic functions. The period of $\zeta^k(t)$ is given by

$$T^k = 4K(k)\sqrt{1-2k^2}.$$

See Fig. 8 for the phase portrait of (4.2).

We apply the subharmonic Melnikov method of [24]. Let $\Omega^k = 2\pi/T^k$ and I^k , respectively, represent the angular frequency and action of $\zeta^k(t)$ (see (3.14)). The Hamiltonian energy for $\zeta^k(t)$ is given by

$$H^k = \frac{k^2(1-k^2)}{(1-2k^2)^2},$$

so that

$$\frac{dH^k}{dk} = \frac{2k}{(1-2k^2)^3} > 0.$$

Since $dH^k/dI^k = \Omega^k > 0$, we have

$$\frac{dI^k}{dk} = \frac{dH^k/dk}{dH^k/dI^k} > 0.$$

We also compute

$$\frac{d\Omega^k}{dk} = -\frac{\pi[(1-2k^2)(E(k)-K(k))-k^2K(k)]}{2k(1-k^2)(1-2k^2)^{3/2}K(k)^2} > 0$$

to obtain

$$\frac{d\Omega^k}{dI^k} = \frac{d\Omega^k/dk}{dI^k/dk} > 0.$$

Let $nT^k = m\hat{T}$ for $m, n > 0$ relatively prime integers. Recall that $\hat{T} = |c/d|\hat{\varepsilon}T$. We compute the subharmonic Melnikov functions as

$$\begin{aligned} M^{m/n}(\phi; \hat{\nu}) &= \int_0^{m\hat{T}} \zeta_2^k(t) [\hat{\nu}\zeta_2^k(t) + s_2\zeta_1^k(t)^2\zeta_2^k(t) + \Delta h(\hat{\omega}t + \phi)] dt \\ &= \hat{\nu}J_1(k, n) + s_2J_2(k, n) + \Delta\hat{h}^{m/n}(\phi) \end{aligned}$$

and

$$L^{m/n}(\phi; \hat{\nu}) = \int_0^{m\hat{T}} (\hat{\nu} + s_2 \zeta_1^k(t)^2) dt = m\hat{\nu}\hat{T} + s_2 J_3(k, n),$$

where

$$\begin{aligned} J_1(k, n) &= \int_0^{m\hat{T}} \zeta_2^k(t)^2 dt = \frac{2k^2}{(1-2k^2)^2} \int_0^{m\hat{T}} \operatorname{sn}^2\left(\frac{t}{\sqrt{1-2k^2}}\right) \operatorname{dn}^2\left(\frac{t}{\sqrt{1-2k^2}}\right) dt \\ &= \frac{8n}{3(1-2k^2)^{3/2}} [(2k^2-1)E(k) + k'^2 K(k)] > 0, \end{aligned}$$

$$\begin{aligned} J_2(k, n) &= \int_0^{m\hat{T}} \zeta_1^k(t)^2 \zeta_2^k(t)^2 dt \\ &= \frac{4k^4}{(1-2k^2)^3} \int_0^{m\hat{T}} \operatorname{dn}^2\left(\frac{t}{\sqrt{1-2k^2}}\right) \operatorname{sn}^2\left(\frac{t}{\sqrt{1-2k^2}}\right) \operatorname{cn}^2\left(\frac{t}{\sqrt{1-2k^2}}\right) dt \\ &= \frac{16n}{15(1-2k^2)^{5/2}} [2(k^4 - k^2 + 1)E(k) - k'^2(2 - k^2)K(k)] > 0, \end{aligned}$$

$$\begin{aligned} J_3(k, n) &= \int_0^{m\hat{T}} \zeta_1^k(t)^2 dt = \frac{2k^2}{1-2k^2} \int_0^{m\hat{T}} \operatorname{cn}^2\left(\frac{t}{\sqrt{1-2k^2}}\right) dt \\ &= \frac{8n}{\sqrt{1-2k^2}} [E(k) - k'^2 K(k)] > 0 \end{aligned}$$

and $\hat{h}^{m/n}(\phi)$ is given by (3.15) with $\zeta_2^k(t)$ of (4.3), for which the statement of Lemma 3.4 also holds. Recall that $k' = \sqrt{1-k^2}$ is complementary elliptic modulus. We prove the following theorem like Theorem 3.5.

Theorem 4.1. *Suppose that $\hat{h}^{m/n}(\phi) \not\equiv 0$ and take ν_1 or ν_2 as a control parameter. Then saddle-node bifurcations of $m\hat{T}$ -periodic (resp. mT -periodic) orbits occur near (3.17) in (4.1) (resp. in (1.2)).*

Remark 4.2. *As in Remark 3.6, one of periodic orbits born at the saddle-node bifurcation detected in Theorem 4.1 is of a sink (resp. a source) type and the other is of a saddle type if condition (3.19) holds, and the former changes its stability from a source type to a sink one or vice versa near (3.20). This suggests that a Hopf bifurcation may occur there.*

Saddle-node bifurcation sets detected by Theorem 4.1 and the behavior of a Poincaré map near $\zeta^k(t)$ with $nT^k = m\hat{T}$ for $(m, n) = (3, 1)$ are similar to those displayed in Fig. 7.

4.2. Case of $\nu_1 > 0$. Let $\hat{\varepsilon}$ be a small positive parameter such that $\nu_1 = \hat{\varepsilon}^2$, and introduce the new state variables $\zeta = (\zeta_1, \zeta_2)$ and the new parameter $\hat{\nu} = O(1)$ as

$$y_1 = \sqrt{\nu_1} \zeta_1, \quad y_2 = \nu_1 \zeta_2, \quad \hat{\nu} = \nu_2 / \nu_1. \quad (4.4)$$

Rescaling the time variable t as $t \rightarrow \sqrt{\nu_1} t$, we rewrite (1.8) as

$$\dot{\zeta}_1 = \zeta_2, \quad \dot{\zeta}_2 = \zeta_1 - \zeta_1^3 + \hat{\varepsilon}(\hat{\nu}\zeta_2 + s_2 \zeta_1^2 \zeta_2 + \Delta h(\hat{\omega}t)), \quad (4.5)$$

where $\hat{\omega}$ and Δ are given by (3.3).

When $\hat{\varepsilon} = 0$, the system (4.5) becomes

$$\dot{\zeta}_1 = \zeta_2, \quad \dot{\zeta}_2 = \zeta_1 - \zeta_1^3 \quad (4.6)$$

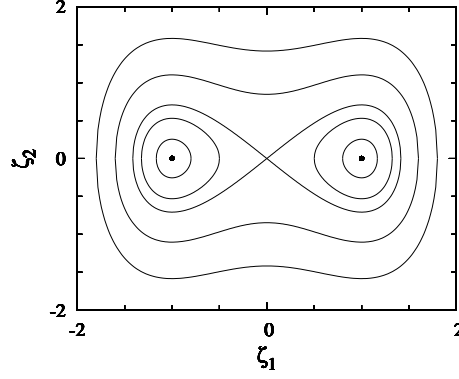


FIGURE 9. Phase portraits of (4.6).

which is a planar Hamiltonian system with the Hamiltonian

$$H(\zeta) = \frac{1}{2}\zeta_2^2 - \frac{1}{2}\zeta_1^2 + \frac{1}{4}\zeta_1^4.$$

The unperturbed system (4.6) has a hyperbolic saddle at the origin to which there exists a pair of homoclinic orbits

$$\zeta_{\pm}^h(t) = \left(\pm\sqrt{2} \operatorname{sech} t, \mp\sqrt{2} \operatorname{sech} t \tanh t \right) \quad (4.7)$$

Moreover, inside each homoclinic orbits, there exists two one-parameter families of periodic orbits,

$$\zeta_{\pm}^k(t) = \left(\pm\sqrt{\frac{2}{2-k^2}} \operatorname{dn} \left(\frac{t}{\sqrt{2-k^2}} \right), \mp\frac{\sqrt{2}k^2}{2-k^2} \operatorname{sn} \left(\frac{t}{\sqrt{2-k^2}} \right) \operatorname{cn} \left(\frac{t}{\sqrt{2-k^2}} \right) \right), \quad k \in (0, 1), \quad (4.8)$$

and outside of the homoclinic orbits, there exists a one-parameter family of periodic orbits,

$$\zeta^k(t) = \left(\frac{\sqrt{2}k}{\sqrt{2k^2-1}} \operatorname{cn} \left(\frac{t}{\sqrt{2k^2-1}} \right), -\frac{\sqrt{2}k}{2k^2-1} \operatorname{sn} \left(\frac{t}{\sqrt{2k^2-1}} \right) \operatorname{dn} \left(\frac{t}{\sqrt{2k^2-1}} \right) \right), \quad k \in (1/\sqrt{2}, 1), \quad (4.9)$$

where k represents the elliptic modulus of the Jacobi's elliptic functions. The periods of $\zeta_{\pm}^k(t)$ and $\zeta^k(t)$ are, respectively, given by

$$T_{\pm}^k = 2K(k)\sqrt{2-k^2} \quad \text{and} \quad T^k = 4K(k)\sqrt{2k^2-1}. \quad (4.10)$$

See Fig. 9 for the phase portrait of (4.6).

4.2.1. *Homoclinic orbits.* We apply the homoclinic Melnikov method [16, 22]. For $\hat{\varepsilon} > 0$ sufficiently small we easily see that the system (4.5) has a hyperbolic periodic orbit near the origin. We compute the Melnikov functions for $\zeta_{\pm}^h(t)$ as

$$\begin{aligned} M_{\pm}(\phi; \hat{\nu}) &= \int_{-\infty}^{\infty} \zeta_{2\pm}^h(t) [\hat{\nu}(\zeta_{2\pm}^h(t)) + s_2 \zeta_{1\pm}^h(t)^2 \zeta_{2\pm}^h(t) + \Delta h(\hat{\omega}t + \phi)] dt \\ &= \frac{4}{3} \hat{\nu} + \frac{16}{15} s_2 \pm \Delta \hat{h}(\phi). \end{aligned}$$

where $\hat{h}(\phi)$ is given by (3.7) with $\zeta_{2+}^h(t)$ of (4.7), for which the statement of Lemma 3.1 also holds. In particular, corresponding to (3.9), we have

$$\tilde{\zeta}_{2+}(\chi) = \int_{-\infty}^{\infty} \zeta_{2+}^h(t) e^{i\chi t} dt = i\pi\chi \operatorname{sech}\left(\frac{\pi\chi}{2}\right) \neq 0$$

for any $\chi \in \mathbb{R}$.

Assume that $h(\phi) \neq 0$. Then the conclusion of Lemma 3.1 holds. If

$$-\hat{h}_{\max} < \frac{4}{3} \hat{\nu} + \frac{16}{15} s_2 < -\hat{h}_{\min}$$

and

$$\hat{h}_{\min} < \frac{4}{3} \hat{\nu} + \frac{16}{15} s_2 < \hat{h}_{\max},$$

i.e.,

$$-\left(\frac{3}{4} \Delta \hat{h}_{\max} + \frac{4}{5} s_2\right) \nu_1 < \nu_2 < -\left(\frac{3}{4} \Delta \hat{h}_{\min} + \frac{4}{5} s_2\right) \nu_1 \quad (4.11)$$

and

$$\left(\frac{3}{4} \Delta \hat{h}_{\min} - \frac{4}{5} s_2\right) \nu_1 < \nu_2 < \left(\frac{3}{4} \Delta \hat{h}_{\max} - \frac{4}{5} s_2\right) \nu_1, \quad (4.12)$$

respectively, then the Melnikov functions $M_{\pm}(\phi)$ cross the zero topologically. Using arguments given in [16, 22], we obtain the following result.

Theorem 4.3. *Suppose that $h(\phi) \neq 0$. If condition (4.11) (resp. (4.12)) holds, then for $|\nu_1|, |\nu_2|, \varepsilon > 0$ sufficiently small the right (resp. left) branches of the stable and unstable manifolds of a periodic orbit near the origin intersect topologically transversely in (4.5) and hence in (1.2). Moreover, homoclinic bifurcations occur near the four curves*

$$\nu_2 = -\left(\frac{3}{4} \Delta \hat{h}_{\max} + \frac{4}{5} s_2\right) \nu_1, \quad \nu_2 = -\left(\frac{3}{4} \Delta \hat{h}_{\min} + \frac{4}{5} s_2\right) \nu_1, \quad \nu_1 > 0. \quad (4.13)$$

$$\nu_2 = \left(\frac{3}{4} \Delta \hat{h}_{\min} - \frac{4}{5} s_2\right) \nu_1, \quad \nu_2 = \left(\frac{3}{4} \Delta \hat{h}_{\max} - \frac{4}{5} s_2\right) \nu_1, \quad \nu_1 > 0. \quad (4.14)$$

Such transverse intersections also yield chaotic dynamics in (4.5) and (1.2) like geometrically transverse intersections, as stated in Remark 3.3.

Figures 10(a) and (b) show the approximate homoclinic bifurcation sets detected by Theorem 4.3 for $s_2 = 1$ and -1 , respectively. The red and blue lines correspond to the bifurcation sets (4.13) and (4.14), respectively. Here we have assumed that $|\hat{h}_{\min}| < |\hat{h}_{\max}|$. Figure 10(c) shows the behavior of the stable and unstable manifolds of periodic orbits near the origin for a Poincaré map in regions ①-⑤ of both figures. In particular, in regions ②-④, there are transverse homoclinic orbits which yield chaotic motions, as stated above. When $|\hat{h}_{\min}| > |\hat{h}_{\max}|$, the loci of the

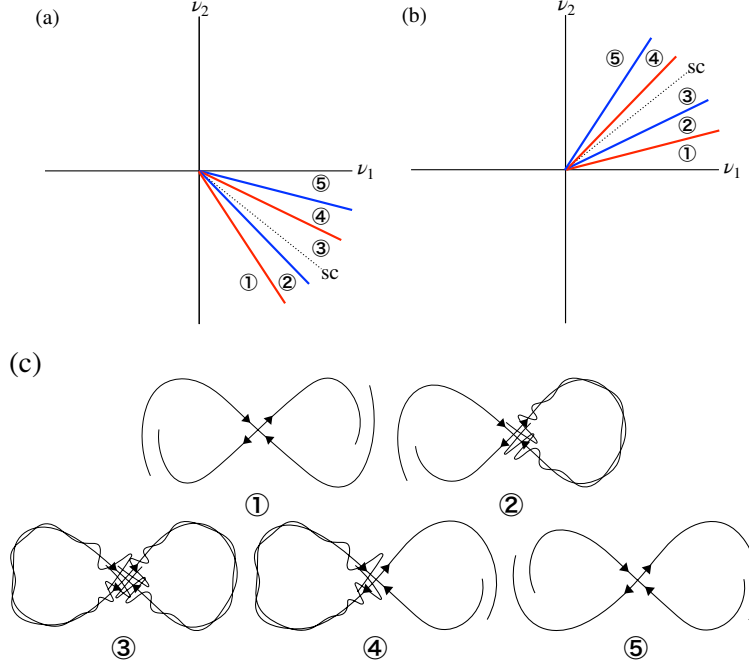


FIGURE 10. Homoclinic bifurcations in (4.5): (a) Approximate bifurcation sets for $s_2 = 1$; (b) for $s_2 = -1$; (c) stable and unstable manifolds for a Poincaré map.

red and blue lines are exchanged in Figs. 10(a) and (b); and when $|\hat{h}_{\min}| = |\hat{h}_{\max}|$, regions ② and ④ disappear or their widths become $o(\sqrt{\nu_1})$.

4.2.2. *Subharmonic orbits.* We apply the subharmonic Melnikov method of [24]. We begin with the families of periodic orbits $\zeta_{\pm}^k(t)$ given by (4.8). Let Ω_{\pm}^k and I_{\pm}^k , respectively, represent the angular frequency and action of $\zeta_{\pm}^k(t)$, where I_{\pm}^k are given by (3.14) with $\zeta^k(t) = \zeta_{\pm}^k(t)$. The Hamiltonian energy for $\zeta_{\pm}^k(t)$ is given by

$$H^k = \frac{k^2 - 1}{(2 - k^2)^2},$$

so that

$$\frac{dH^k}{dk} = \frac{2k^3}{(2 - k^2)^3} > 0.$$

Since $dH^k/dI_{\pm}^k = \Omega_{\pm}^k > 0$ and

$$\frac{d}{dk} [(2 - k^2)E(k) - 2(1 - k^2)K(k)] = -3k[E(k) - K(k)] > 0,$$

we have

$$\frac{dI_{\pm}^k}{dk} = \frac{dH^k/dk}{dH^k/dI_{\pm}^k} > 0$$

and

$$\frac{d\Omega_{\pm}^k}{dk} = -\frac{\pi[(2-k^2)E(k) - 2(1-k^2)K(k)]}{k(2-k^2)^{3/2}(1-k^2)K(k)} < 0.$$

Hence,

$$\frac{d\Omega_{\pm}^k}{dI_{\pm}^k} = \frac{d\Omega_{\pm}^k/dk}{dI_{\pm}^k/dk} < 0.$$

Let $nT^k = m\hat{T}$ for $m, n > 0$ relatively prime integers. Recall that $\hat{T} = |c/d|\hat{\varepsilon}T$. We compute the subharmonic Melnikov functions as

$$\begin{aligned} M_{\pm}^{m/n}(\phi; \hat{\nu}) &= \int_0^{m\hat{T}} \zeta_{2\pm}^k(t) [\hat{\nu}\zeta_{2\pm}^k(t) + s_2\zeta_{1\pm}^k(t)^2\zeta_{2\pm}^k(t) + \Delta h(\hat{\omega}t + \phi)] dt \\ &= \hat{\nu}J_1(k, n) + s_2J_2(k, n) \pm \Delta\hat{h}^{m/n}(\phi) \end{aligned}$$

and

$$L_{\pm}^{m/n}(\phi; \hat{\nu}) = \int_0^{m\hat{T}} (\hat{\nu} + s_2\zeta_{1\pm}^k(t)^2) dt = m\hat{\nu}\hat{T} + s_2J_3(k, n),$$

where

$$\begin{aligned} J_1(k, n) &= \int_0^{m\hat{T}} (\zeta_{2\pm}^k(t))^2 dt = \frac{2k^4}{(2-k^2)^2} \int_0^{m\hat{T}} \operatorname{sn}^2\left(\frac{t}{\sqrt{2-k^2}}\right) \operatorname{cn}^2\left(\frac{t}{\sqrt{2-k^2}}\right) dt \\ &= \frac{4n}{3(2-k^2)^{3/2}} [(2-k^2)E(k) - k'^2K(k)], \end{aligned}$$

$$\begin{aligned} J_2(k, n) &= \int_0^{m\hat{T}} \zeta_{1\pm}^k(t)^2\zeta_{2\pm}^k(t)^2 dt \\ &= \frac{4k^4}{(2-k^2)^3} \int_0^{m\hat{T}} \operatorname{dn}^2\left(\frac{t}{\sqrt{2-k^2}}\right) \operatorname{sn}^2\left(\frac{t}{\sqrt{2-k^2}}\right) \operatorname{cn}^2\left(\frac{t}{\sqrt{2-k^2}}\right) dt \\ &= \frac{8n}{15(2-k^2)^{5/2}} [2(k^4 - k^2 + 1)E(k) - k'^2(2-k^2)K(k)], \end{aligned}$$

$$J_3(k, n) = \int_0^{m\hat{T}} \zeta_{1\pm}^k(t)^2 dt = \frac{2}{2-k^2} \int_0^{m\hat{T}} \operatorname{dn}^2\left(\frac{t}{\sqrt{2-k^2}}\right) dt = \frac{4nE(k)}{\sqrt{2-k^2}}$$

and $\hat{h}^{m/n}(\phi)$ is given by (3.15) with $\zeta_2^k(t) = \zeta_{2+}^k(t)$, for which the statement of Lemma 3.4 also holds. Recall that $k' = \sqrt{1-k^2}$ is complementary elliptic modulus. We prove the following theorem like Theorems 3.5 and 4.1.

Theorem 4.4. *Suppose that $\hat{h}^{m/n}(\phi) \not\equiv 0$ and take ν_1 or ν_2 as a control parameter. Then saddle-node bifurcations of $m\hat{T}$ -periodic (resp. mT -periodic) orbits near the unperturbed periodic orbits with $\zeta_1 > 0$ and with $\zeta_1 < 0$ occur near the curves*

$$\nu_2 = -\frac{\Delta\hat{h}_{\max}^{m/n} + s_2J_2(k, n)}{J_1(k, n)}\nu_1, \quad \nu_2 = -\frac{\Delta\hat{h}_{\min}^{m/n} + s_2J_2(k, n)}{J_1(k, n)}\nu_1, \quad \nu_1 > 0, \quad (4.15)$$

and

$$\nu_2 = \frac{\Delta\hat{h}_{\min}^{m/n} - s_2J_2(k, n)}{J_1(k, n)}\nu_1, \quad \nu_2 = \frac{\Delta\hat{h}_{\max}^{m/n} - s_2J_2(k, n)}{J_1(k, n)}\nu_1, \quad \nu_1 > 0, \quad (4.16)$$

in (4.5) (resp. in (1.2)), respectively.

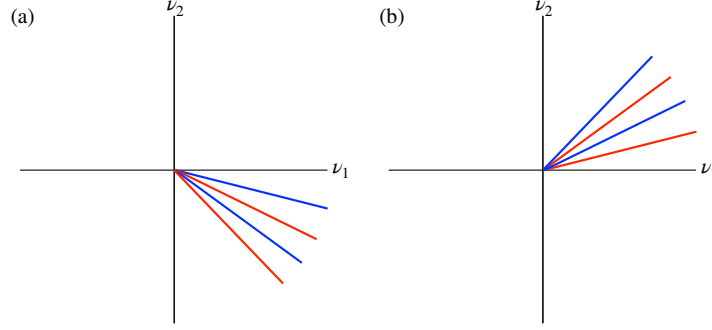


FIGURE 11. Saddle-node bifurcations in (4.5): (a) Approximate bifurcation sets for $s_2 = 1$; (b) for $s_2 = -1$.

Figures 11(a) and (b) show the approximate saddle-node bifurcation sets detected by Theorem 4.4 for $s_2 = 1$ and -1 , respectively. Here we have assumed that $|\hat{h}_{\min}| < |\hat{h}_{\max}|$. The red and blue lines correspond to the bifurcation sets (4.15) and (4.16), respectively. The behavior of a Poincaré map near the resonant periodic orbit $\zeta_+^k(t)$ (resp. near $\zeta_-^k(t)$) with $nT_+^k = m\hat{T}$ (resp. with $nT_-^k = m\hat{T}$) for $(m, n) = (3, 1)$ in the regions between the two red lines (resp. the two blue lines) in Figs. 11(a) and (b) is similar to that displayed in Figure 7(c). When $|\hat{h}_{\min}| > |\hat{h}_{\max}|$, the loci of the red and blue lines are exchanged in Figs. 11(a) and (b).

We turn to the family of periodic orbits $\zeta^k(t)$ given by (4.9). Let $\Omega^k = 2\pi/T^k$ and I^k , respectively, represent the angular frequency and action of $\zeta^k(t)$, where I^k is given by (3.14). The Hamiltonian energy for $\zeta^k(t)$ is given by

$$H^k = \frac{k^2(1 - k^2)}{(2k^2 - 1)^2},$$

so that

$$\frac{dH^k}{dk} = -\frac{2k}{(2k^2 - 1)^3} < 0.$$

Since $dH^k/dI^k = \Omega_{\pm}^k = 2\pi/T^k > 0$, we have

$$\frac{dI^k}{dk} = \frac{dH^k/dk}{dH^k/dI^k} < 0$$

and

$$\frac{d\Omega^k}{dk} = -\frac{\pi[(1 - k^2)(K(k) - E(k)) + k^2E(k)]}{2k(1 - k^2)(2k^2 - 1)^{3/2}K(k)^2} < 0.$$

Hence,

$$\frac{d\Omega^k}{dI^k} = \frac{d\Omega^k/dk}{dI^k/dk} > 0.$$

Let $nT^k = m\hat{T}$ for $m, n > 0$ relatively prime integers. Recall that $\hat{T} = |c/d|\hat{\varepsilon}T$. We compute the subharmonic Melnikov functions as

$$\begin{aligned} M^{m/n}(\phi; \hat{\nu}) &= \int_0^{m\hat{T}} \zeta_2^k(t) [\hat{\nu}\zeta_2^k(t) + s_2\zeta_1^k(t)^2\zeta_2^k(t) + \Delta h(\hat{\omega}t + \phi)] dt \\ &= \hat{\nu}J_1(k, n) + s_2J_2(k, n) + \Delta\hat{h}^{m/n}(\phi) \end{aligned}$$

and

$$L^{m/n}(\phi; \hat{\nu}) = \int_0^{m\hat{T}} (\hat{\nu} + s_2\zeta_1^k(t)^2) dt = m\hat{\nu}\hat{T} + s_2J_3(k, n),$$

where

$$\begin{aligned} J_1(k, n) &= \int_0^{m\hat{T}} \zeta_2^k(t)^2 dt = \frac{2k^2}{(2k^2-1)^2} \int_0^{m\hat{T}} \operatorname{sn}^2\left(\frac{t}{\sqrt{2k^2-1}}\right) \operatorname{dn}^2\left(\frac{t}{\sqrt{2k^2-1}}\right) dt \\ &= \frac{8n}{3(2k^2-1)^{3/2}} [(2k^2-1)E(k) + k'^2K(k)] > 0, \\ J_2(k, n) &= \int_0^{m\hat{T}} \zeta_1^k(t)^2\zeta_2^k(t)^2 dt \\ &= \frac{4k^4}{(2k^2-1)^3} \int_0^{m\hat{T}} \operatorname{dn}^2\left(\frac{t}{\sqrt{2k^2-1}}\right) \operatorname{sn}^2\left(\frac{t}{\sqrt{2k^2-1}}\right) \operatorname{cn}^2\left(\frac{t}{\sqrt{2k^2-1}}\right) dt \\ &= \frac{16n}{15(2k^2-1)^{5/2}} [2(k^4-k^2+1)E(k) - k'^2(2-k^2)K(k)] > 0, \\ J_3(k, n) &= \int_0^{m\hat{T}} \zeta_1^k(t)^2 dt = \frac{2k^2}{2k^2-1} \int_0^{m\hat{T}} \operatorname{cn}^2\left(\frac{t}{\sqrt{2k^2-1}}\right) dt \\ &= \frac{8n}{\sqrt{2k^2-1}} [E(k) - k'^2K(k)] > 0 \end{aligned}$$

and $\hat{h}^{m/n}(\phi)$ is given by (3.15) with $\zeta_2^k(t)$ of (4.9), for which the statement of Lemma 3.4 also holds. We prove the following theorem like Theorems 3.5, 4.1 and 4.4.

Theorem 4.5. *Suppose that $\hat{h}^{m/n}(\phi) \not\equiv 0$ and take ν_1 or ν_2 as a control parameter. Then saddle-node bifurcations of $m\hat{T}$ -periodic (resp. mT -periodic) orbits occur near*

$$\nu_2 = -\frac{\Delta\hat{h}_{\max} + s_2J_2(k, n)}{J_1(k, n)}\nu_1 \quad \text{and} \quad \nu_2 = -\frac{\Delta\hat{h}_{\min} + s_2J_2(k, n)}{J_1(k, n)}\nu_1, \quad \nu_1 > 0 \quad (4.17)$$

in (4.5) (resp. in (1.2)).

Remark 4.6. *As in Remarks 3.6 and 4.2, one of periodic orbits born at the saddle-node bifurcations detected in Theorem 4.4 or 4.5 is of a sink (resp. a source) type and the other is of a saddle type if*

$$m\hat{\nu}\hat{T} + s_2J_3(k, n) < 0 \quad (\text{resp. } > 0),$$

i.e.,

$$\nu_2 < -\frac{s_2J_3(k, n)}{m\hat{T}}\nu_1 \quad \left(\text{resp. } \nu_2 > -\frac{s_2J_3(k, n)}{m\hat{T}}\nu_1 \right),$$

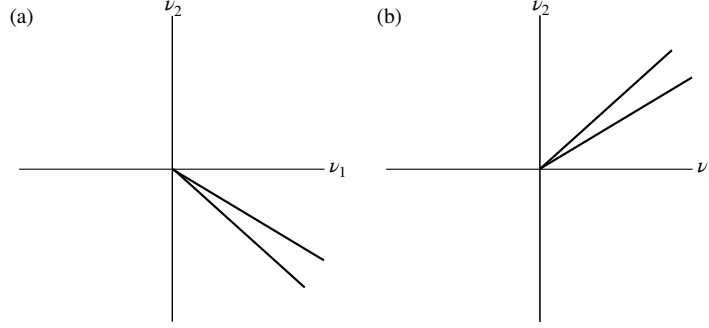


FIGURE 12. Saddle-node bifurcations of (4.5): (a) Approximate bifurcation sets for $s_2 = 1$; (b) for $s_2 = -1$.

and the former changes its stability from a source type to a sink one or vice versa near

$$\nu_2 = -\frac{s_2 J_3(k, n)}{m\hat{T}} \nu_1, \quad \nu_1 > 0.$$

This suggests that a Hopf bifurcation may occur there.

Figures 12(a) and (b) show the approximate saddle-node bifurcation sets detected by Theorem 4.5 for $s_2 = 1$ and -1 , respectively. The behavior of a Poincaré map near the resonant periodic orbit $\zeta^k(t)$ with $nT_+^k = m\hat{T}$ for $(m, n) = (3, 1)$ is similar to that displayed in Fig. 7(c).

5. HIGHER-DIMENSIONAL SYSTEMS

Let $\varepsilon > 0$ be a small parameter and let $\omega > 0$ be a constant, as in the previous sections. Consider $(d + 2)$ -dimensional systems of the form

$$\begin{aligned} \dot{u} &= Ju + f_u(u, v; \mu) + \varepsilon g_u(u, v, \omega t), \\ \dot{v} &= Av + f_v(u, v; \mu) + \varepsilon g_v(u, v, \omega t), \end{aligned} \quad (u, v) \in \mathbb{R}^2 \times \mathbb{R}^d, \quad (5.1)$$

with a control parameter vector $\mu \in \mathbb{R}^2$, where A is an $n \times n$ matrix of which all eigenvalues have nonzero real parts, $f_u : \mathbb{R}^2 \times \mathbb{R}^d \times \mathbb{R}^2 \rightarrow \mathbb{R}^2$ and $f_v : \mathbb{R}^2 \times \mathbb{R}^d \times \mathbb{R}^2 \rightarrow \mathbb{R}^d$ are C^4 and symmetric around $(u, v) = (0, 0)$, i.e.,

$$f_u(-u, -v; \mu) = -f_u(u, v; \mu), \quad f_v(-u, -v; \mu) = -f_v(u, v; \mu), \quad (5.2)$$

with $f_u(u, v; \mu), f_v(u, v; \mu) = O(|u|^3 + |v|^3 + |\mu|(|u| + |v|))$, $g_u : \mathbb{R}^2 \times \mathbb{R}^d \times \mathbb{R} \rightarrow \mathbb{R}^2$ and $g_v : \mathbb{R}^2 \times \mathbb{R}^d \times \mathbb{R} \rightarrow \mathbb{R}^d$ are C^2 , and $g_u(u, v, \phi)$ and $g_v(u, v, \phi)$ have mean zero in ϕ for any $(u, v) \in \mathbb{R}^2 \times \mathbb{R}^d$. In particular, $(u, v) = (0, 0)$ is an equilibrium in (5.1) for $\mu \neq 0$ since by (5.2)

$$f_u(0, 0; \mu) = f_v(0, 0; \mu) = 0.$$

Recall that J is the Jordan normal form given by (1.5). We extend (5.1) to the $(d + 5)$ -dimensional system

$$\begin{aligned} \dot{u} &= Ju + f_u(u, v; \mu) + \varepsilon g_u(u, v, \phi), \\ \dot{v} &= Av + f_v(u, v; \mu) + \varepsilon g_v(u, v, \phi), \\ \dot{\phi} &= \omega, \quad \dot{\mu} = 0 \end{aligned} \quad (5.3)$$

in $\mathbb{R}^2 \times \mathbb{R}^d \times \mathbb{S}^1 \times \mathbb{R}^2$.

When $\varepsilon = 0$, the system (5.3) has a one-dimensional invariant manifold

$$\mathcal{M} = \{(u, v, \phi, \mu) \mid (u, v, \mu) = (0, 0, 0), \phi \in \mathbb{S}^1\}$$

for which there is a five-dimensional center manifold

$$W^c(\mathcal{M}) = \{(u, v, \phi, \mu) \mid v = \bar{v}(u, \mu), \phi \in \mathbb{S}^1, \mu \in U_0\}$$

near \mathcal{M} , where $\bar{v}(u, \mu) = O(|u|^3 + |\mu||u|)$ and $U_0 \subset \mathbb{R}^2$ is a neighborhood of $\mu = 0$. The dynamics of (5.3) with $\varepsilon = 0$ on $W^c(\mathcal{M})$ are governed by

$$\dot{u} = Ju + f_u(u, 0; \mu) + O(|u|^5 + |\mu||u|^3), \quad \dot{\phi} = \omega, \quad \dot{\mu} = 0$$

since

$$f_u(u, \bar{v}(u; \mu); \mu) = f_u(u, 0; \mu) + O(|u|^5 + |\mu||u|^3).$$

See [8, 16–18, 22] for the general approach of center manifold reduction. $\mathcal{N}_0 = W^c(\mathcal{M})$ is also a normally hyperbolic, locally invariant manifold [13–15, 21].

Let $\varepsilon > 0$. From the invariant manifold theory of Fenichel [14, 15] (see also [13, 21]) we show that there exists a five-dimensional normally hyperbolic, locally invariant manifold

$$\mathcal{N}_\varepsilon = \{(u, v, \phi, \mu) \mid v = \bar{v}(u, \mu) + \varepsilon \tilde{v}(u, \phi, \mu), \phi \in \mathbb{S}^1, \mu \in U\}$$

near \mathcal{N}_0 , where $U \subset U_0$ is a neighborhood of $\mu = 0$. The dynamics of (5.3) on \mathcal{N}_ε are governed by

$$\begin{aligned} \dot{u} &= Ju + f_u(u, \bar{v}(u, \mu) + \varepsilon \tilde{v}(u, \phi, \mu); \mu) + \varepsilon g_u(u, \bar{v}(u, \mu) + \varepsilon \tilde{v}(u, \phi, \mu), \phi), \\ \dot{\phi} &= \omega, \quad \dot{\mu} = 0. \end{aligned} \tag{5.4}$$

Here we have

$$\begin{aligned} f_u(u, \bar{v}(u, \mu) + \varepsilon \tilde{v}(u, \phi, \mu); \mu) &= f_u(u, 0; \mu) + O(|u|^5 + |\mu||u|^3 + \varepsilon|u|^2), \\ g_u(u, \bar{v}(u, \mu) + \varepsilon \tilde{v}(u, \phi, \mu), \phi) &= g_u(u, 0, \phi) + O(|u|^3 + \varepsilon) \end{aligned}$$

by assumption. Hence, letting $\phi = \omega t$, we rewrite the first equation of (5.4) as

$$\dot{u} = Ju + f_u(u, 0; \mu) + \varepsilon g_u(u, 0, \omega t) + O(|u|^5 + |\mu||u|^3 + \varepsilon|u|^2 + \varepsilon^2). \tag{5.5}$$

We eliminate the higher-order terms in (5.5), and apply the arguments of Section 2 to obtain (1.8).

6. EXAMPLE

We apply our theory to the three-dimensional system (1.1) with (1.7). Henceforth we assume that $\theta_0 = 0$ or π and that $\delta_1 \neq \pm 1$. Recall that $\alpha, \delta_0 > 0$. Following the approach of [27] basically, we first obtain a two-dimensional system of the form (1.8) governing its dynamics approximately on the locally invariant manifold \mathcal{N}_ε .

6.1. Center manifold reduction. Let $\varepsilon = 0$ in (1.7), i.e., $\theta_d = \theta_0 (= 0 \text{ or } \pi)$. The system (1.1) has an equilibrium at $z = (\theta_d, 0, 0)$ and its right hand side has the Jacobian matrix

$$\begin{pmatrix} 0 & 1 & 0 \\ -\sigma & -\delta_0 & 1 \\ -\gamma & -\delta_1 & -\alpha \end{pmatrix} \tag{6.1}$$

at the equilibrium, where $\sigma = 1$ if $\theta_0 = 0$ and $\sigma = -1$ if $\theta_d = \pi$. So we easily see that the matrix (6.1) has a double zero when

$$\alpha\delta_0 + \delta_1 + \sigma = 0, \quad \gamma = -\sigma\alpha \quad (6.2)$$

(see Section 3 of [27]). Let

$$\alpha_0 = -\frac{\sigma + \delta_1}{\delta_0}, \quad \gamma_0 = \frac{\sigma(\sigma + \delta_1)}{\delta_0}, \quad (6.3)$$

so that $\alpha = \alpha_0$ and $\gamma = \gamma_0$ satisfy (6.2). The system (1.1) with $\theta_d = 0$ or π possesses a symmetry about $z = (0, 0, 0)$ or $(\pi, 0, 0)$, i.e., it is invariant under the transformation

$$(z_1, z_2, z_3) \mapsto (-z_1, -z_2, -z_3) \quad \text{or} \quad (z_1 - \pi, z_2, z_3) \mapsto (\pi - z_1, -z_2, -z_3).$$

We now set $\beta > 0$. Letting

$$\tilde{z}_1 = z_1 - \theta_0, \quad \tilde{z}_j = z_j, \quad j = 2, 3,$$

we rewrite (1.1) as

$$\begin{pmatrix} \dot{\tilde{z}}_1 \\ \dot{\tilde{z}}_2 \\ \dot{\tilde{z}}_3 \end{pmatrix} = \begin{pmatrix} 0 & 1 & 0 \\ -\sigma & -\delta_0 & 1 \\ -(\gamma_0 + \gamma_1) & -\delta_1 & -(\alpha_0 + \alpha_1) \end{pmatrix} \begin{pmatrix} \tilde{z}_1 \\ \tilde{z}_2 \\ \tilde{z}_3 \end{pmatrix} + \begin{pmatrix} 0 \\ \frac{1}{6}\sigma\tilde{z}_1^3 \\ \varepsilon\beta\gamma_0 \cos \omega t \end{pmatrix} + \text{h.o.t.}, \quad (6.4)$$

where $\alpha_1 = \alpha - \alpha_0$ and $\gamma_1 = \gamma - \gamma_0$. Using the change of the coordinates

$$\begin{pmatrix} \tilde{z}_1 \\ \tilde{z}_2 \\ \tilde{z}_3 \end{pmatrix} = \begin{pmatrix} 1 & 0 & \delta_0 \\ 0 & 1 & -\delta_0(\alpha_0 + \delta_0) \\ \sigma & \delta_0 & -\delta_1(\alpha_0 + \delta_0) + \gamma_0 \end{pmatrix} \begin{pmatrix} u_1 \\ u_2 \\ v \end{pmatrix}$$

in (6.4), we have

$$\begin{pmatrix} \dot{u}_1 \\ \dot{u}_2 \\ \dot{v} \end{pmatrix} = \begin{pmatrix} \tilde{a}_{11}\alpha_1 + \tilde{b}_{11}\gamma_1 & 1 + \tilde{a}_{12}\alpha_1 & \tilde{a}_{13}\alpha_1 + \tilde{b}_{13}\gamma_1 \\ \tilde{a}_{21}\alpha_1 + \tilde{b}_{21}\gamma_1 & \tilde{a}_{22}\alpha_1 & \tilde{a}_{23}\alpha_1 + \tilde{b}_{23}\gamma_1 \\ \tilde{a}_{31}\alpha_1 + \tilde{b}_{31}\gamma_1 & \tilde{a}_{32}\alpha_1 & -(\alpha_0 + \delta_0) + \tilde{a}_{33}\alpha_1 + \tilde{b}_{33}\gamma_1 \end{pmatrix} \begin{pmatrix} u_1 \\ u_2 \\ v \end{pmatrix} + \begin{pmatrix} \frac{\sigma\delta_0(u_1 + \delta_0v)^3}{6(\alpha_0 + \delta_0)^2} \\ \frac{\sigma\alpha_0(u_1 + \delta_0v)^3}{6(\alpha_0 + \delta_0)} \\ -\frac{\sigma(u_1 + \delta_0v)^3}{6(\alpha_0 + \delta_0)^2} \end{pmatrix} - \varepsilon\beta\gamma_0 \cos \omega t \begin{pmatrix} \tilde{b}_{11} \\ \tilde{b}_{21} \\ \tilde{b}_{31} \end{pmatrix}, \quad (6.5)$$

where

$$\begin{aligned}
\tilde{a}_{11} &= \frac{\sigma}{(\alpha_0 + \delta_0)^2}, & \tilde{a}_{12} &= \frac{\delta_0}{(\alpha_0 + \delta_0)^2}, & \tilde{a}_{13} &= \frac{\delta_0(\alpha_0^2 - \delta_1)}{(\alpha_0 + \delta_0)^2}, \\
\tilde{a}_{21} &= -\frac{\sigma}{\alpha_0 + \delta_0}, & \tilde{a}_{22} &= -\frac{\delta_0}{\alpha_0 + \delta_0}, & \tilde{a}_{23} &= -\frac{\delta_0(\alpha_0^2 - \delta_1)}{\alpha_0 + \delta_0}, \\
\tilde{a}_{31} &= -\frac{\sigma}{\delta_0(\alpha_0 + \delta_0)^2}, & \tilde{a}_{32} &= -\frac{1}{(\alpha_0 + \delta_0)^2}, & \tilde{a}_{33} &= -\frac{\alpha_0^2 - \delta_1}{\delta_0(\alpha_0 + \delta_0)^2}, \\
\tilde{b}_{11} &= \frac{1}{(\alpha_0 + \delta_0)^2}, & \tilde{b}_{13} &= \frac{\delta_0}{(\alpha_0 + \delta_0)^2}, & \tilde{b}_{21} &= -\frac{1}{\alpha_0 + \delta_0}, \\
\tilde{b}_{23} &= -\frac{\delta_0}{\alpha_0 + \delta_0}, & \tilde{b}_{31} &= -\frac{1}{\delta_0(\alpha_0 + \delta_0)^2}, & \tilde{b}_{33} &= -\frac{1}{(\alpha_0 + \delta_0)^2}.
\end{aligned}$$

The system (6.5) has the form (5.1) with $A = -(\alpha_0 + \delta_0)$. So we obtain (5.5) without the higher-order terms as

$$\begin{aligned}
\begin{pmatrix} \dot{u}_1 \\ \dot{u}_2 \end{pmatrix} &= J \begin{pmatrix} u_1 \\ u_2 \end{pmatrix} + \begin{pmatrix} \frac{\sigma\delta_0 u_1^3}{6(\alpha_0 + \delta_0)^2} \\ \frac{\sigma\alpha_0 u_1^3}{6(\alpha_0 + \delta_0)} \end{pmatrix} \\
&+ \begin{pmatrix} (\tilde{a}_{11}\alpha_1 + \tilde{b}_{11}\gamma_1)u_1 + \tilde{a}_{12}\alpha_1 u_2 \\ (\tilde{a}_{21}\alpha_1 + \tilde{b}_{21}\gamma_1)u_1 + \tilde{a}_{22}\alpha_1 u_2 \end{pmatrix} - \varepsilon\beta\gamma_0 \cos \omega t \begin{pmatrix} \tilde{b}_{11} \\ \tilde{b}_{21} \end{pmatrix}. \quad (6.6)
\end{aligned}$$

We now apply the arguments of Section 2. The system (6.5) has the form (1.2) with $x = (u_1, u_2)$ and $\mu = (\alpha_1, \gamma_1)$, where $f(x; \mu)$ is given by (2.1) with

$$\begin{aligned}
a_{130} &= \frac{\sigma\delta_0}{(\alpha_0 + \delta_0)^2}, & a_{230} &= \frac{\sigma\alpha_0}{\alpha_0 + \delta_0}, & a_{jkl} &= 0, & j &= 1, 2, & \text{for } (k, l) \neq (3, 0), \\
b_{j1k} &= \tilde{a}_{jk}, & b_{j12} &= \tilde{b}_{j1}, & b_{j22} &= 0, & j, k &= 1, 2,
\end{aligned}$$

and

$$g(x, \phi) = -\beta\gamma_0 \cos \phi \begin{pmatrix} \tilde{b}_{11} \\ \tilde{b}_{21} \end{pmatrix}.$$

We easily see that conditions (1.6) and (2.2) hold, where

$$c = \frac{\sigma\alpha_0}{6(\alpha_0 + \delta_0)}, \quad d = \frac{\sigma\delta_0}{2(\alpha_0 + \delta_0)^2}.$$

Equations (2.6) and (2.7) become

$$\begin{aligned}
\nu_1 &= \frac{9\delta_0^2(\tilde{a}_{21}\alpha_1 + \tilde{b}_{21}\gamma_1)}{\alpha_0^2(\alpha_0 + \delta_0)^2}, & \nu_2 &= \frac{3\delta_0((\tilde{a}_{11} + \tilde{a}_{22})\alpha_1 + \tilde{b}_{11}\gamma_1)}{\alpha_0(\alpha_0 + \delta_0)}, \\
s_1, s_2 &= \text{sign}(\sigma), & \bar{\omega} &= \frac{3\delta_0\omega}{\alpha_0(\alpha_0 + \delta_0)}
\end{aligned} \quad (6.7)$$

and

$$h(\phi) = \frac{9\sqrt{6}\beta\gamma_0\delta_0^3}{2\alpha_0^{5/2}(\alpha_0 + \delta_0)^{9/2}} \cos \phi,$$

respectively. We have $s_1, s_2 = 1$ or $s_1, s_2 = -1$ depending on whether $\sigma = 1$ or -1 , i.e., $\theta_0 = 0$ or π , since $\alpha_0, \delta_0 > 0$.

6.2. **Case of $\theta_0 = 0$.** We begin with the case of $\theta_0 = 0$, in which $\sigma = 1$ and $s_1, s_2 = 1$. Let $\nu_1 = -\hat{\varepsilon}^2$ and define $\hat{\omega}, \Delta$ as in (3.3). We compute (3.7) for (3.5) as

$$\begin{aligned}\hat{h}(\phi) &= \pm \frac{9\sqrt{3}\beta\gamma_0\delta_0^3}{2\alpha_0^{5/2}(\alpha_0 + \delta_0)^{9/2}} \int_{-\infty}^{\infty} \operatorname{sech}^2\left(\frac{t}{\sqrt{2}}\right) \cos(\hat{\omega}t + \phi) dt \\ &= \pm \frac{9\sqrt{3}\pi\beta\gamma_0\delta_0^3\hat{\omega}}{\alpha_0^{5/2}(\alpha_0 + \delta_0)^{9/2}} \operatorname{csch}\left(\frac{\pi\hat{\omega}}{\sqrt{2}}\right) \cos\phi\end{aligned}$$

and (3.15) for (3.6) as

$$\begin{aligned}\hat{h}^{m/n}(\phi) &= \frac{9\sqrt{3}k\beta\gamma_0\delta_0^3}{\alpha_0^{5/2}(\alpha_0 + \delta_0)^{9/2}(k^2 + 1)} \\ &\quad \times \int_0^{m\hat{T}} \operatorname{cn}\left(\frac{t}{\sqrt{k^2 + 1}}\right) \operatorname{dn}\left(\frac{t}{\sqrt{k^2 + 1}}\right) \cos(\hat{\omega}t + \phi) dt \\ &= \begin{cases} \frac{18\sqrt{3}\pi\beta\gamma_0\delta_0^3\hat{\omega}}{\alpha_0^{5/2}(\alpha_0 + \delta_0)^{9/2}} \operatorname{csch}\left(\frac{m\pi K(k')}{2K(k)}\right) \cos\phi & \text{if } m \text{ is odd and } n = 1; \\ 0 & \text{otherwise,} \end{cases}\end{aligned}$$

where the resonance relation $nT^k = m\hat{T} = 2m\pi/\hat{\omega}$ has been used. Note that by (6.3) $\gamma_0 < 0$ since $\alpha_0, \delta_0 > 0$. Using Theorems 3.2 and 3.5 and Remark 3.6, we obtain the following.

Proposition 6.1. *Let $\theta_0 = 0$. There exist two periodic orbits near $z = (\pm\sqrt{-\nu_1}, 0, 0)$ in (1.1) with (1.7) such that the left branch of the stable (resp. unstable) manifold of the right periodic orbit intersect the right branch of the unstable (resp. stable) manifold of the left periodic orbit transversely if for $|\nu_1|, |\nu_2|, \varepsilon > 0$ sufficiently small condition (3.10) holds with*

$$\hat{h}_{\max} = -\frac{9\sqrt{3}\pi\beta\gamma_0\delta_0^3\hat{\omega}}{\alpha_0^{5/2}(\alpha_0 + \delta_0)^{9/2}} \operatorname{csch}\left(\frac{\pi\hat{\omega}}{\sqrt{2}}\right), \quad \hat{h}_{\min} = -\hat{h}_{\max}.$$

Moreover, heteroclinic bifurcations occur near the two curves given by (3.12) or equivalently by (3.13).

Proposition 6.2. *Let $\theta_0 = 0$ and let $m > 0$ be an odd integer. Then saddle-node bifurcations of $2m\pi/\omega$ -periodic orbits around the origin occur in (1.1) with (1.7) near the two curves given by (3.17) with*

$$\hat{h}_{\max}^{m/1} = -\frac{18\sqrt{3}\pi\beta\gamma_0\delta_0^3\hat{\omega}}{\alpha_0^{5/2}(\alpha_0 + \delta_0)^{9/2}} \operatorname{csch}\left(\frac{m\pi K(k')}{2K(k)}\right), \quad \hat{h}_{\min}^{m/1} = -\hat{h}_{\max}^{m/1}.$$

Moreover, one of the periodic orbits born at the bifurcations is of a sink or saddle type, depending on whether

$$\hat{h}_{\max}^{m/1}, \hat{h}_{\min}^{m/1} > -\frac{1}{\Delta} \left(\frac{J_1(k, 1)J_3(k, 1)}{m\hat{T}} - J_2(k, 1) \right) \quad (6.8)$$

or the opposite of inequality holds, while the other is always a saddle.

The dependence of \hat{h}_{\max} and $\hat{h}_{\max}^{m/1}$ on $\hat{\omega}$ when $\alpha_0 = 1$, $\gamma_0 = -1$, $\delta_0 = 0.2$ and $\Delta = 1$ is shown for $m = 1, 3, 5, 7, 9$ in Fig. 13. Condition (6.8) holds for \hat{h}_{\min} , i.e., one of the periodic orbits born at the saddle-node bifurcation given by the second

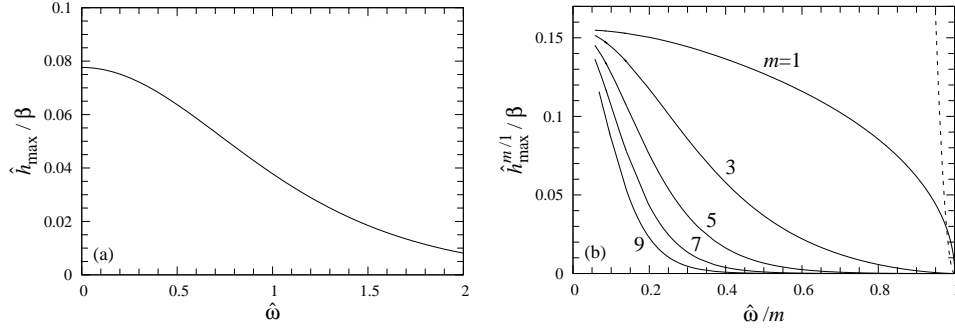


FIGURE 13. Dependence of \hat{h}_{max} and $\hat{h}_{max}^{m/1}$ on $\hat{\omega}$ for $\alpha_0 = 1$, $\gamma_0 = -1$ and $\delta_0 = 0.2$ in Propositions 6.1 and 6.2: (a) \hat{h}_{max} ; (b) $\hat{h}_{max}^{m/1}$ for $m = 1, 3, 5, 7, 9$. Condition (6.8) holds for \hat{h}_{min} below the broken line in Fig. (b).

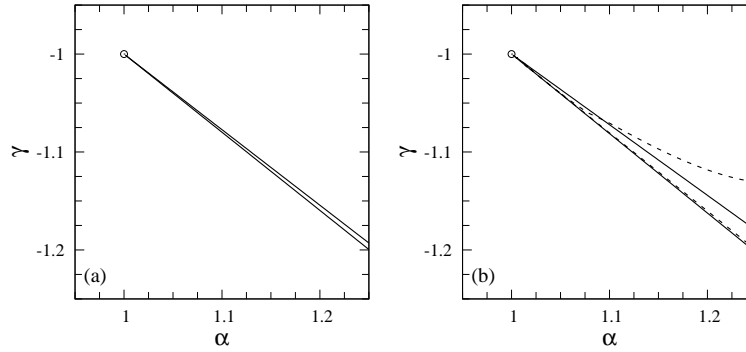


FIGURE 14. Bifurcation sets in (1.1) with (1.7) for $\theta_0 = 0$, $\delta_0 = 0.2$, $\delta_1 = -1.2$, $\beta = 5$ and $\hat{\omega} = 0.8$: (a) Heteroclinic bifurcations for $\hat{\omega} = 1.4$; (b) saddle-node bifurcations for $\hat{\omega} = 0.8$ and $m = 1$. The circle represents the codimension-two bifurcation point. The solid and broken lines, respectively, represent the theoretical predictions and numerical results in Fig. (b).

equation of (3.17) is of a sink type, below the broken line in Fig. 13(b), while it always holds for \hat{h}_{max} .

Henceforth we fix $\delta_0 = 0.2$, $\delta_1 = -1.2$, $\beta = 0.5$, $\Delta = 1$, and $\hat{\omega} = 0.8$ or 1.4 , so that $\alpha_0 = 1$ and $\gamma_0 = -1$, and give numerical results to demonstrate the above theoretical ones. The values of ε , $\hat{\varepsilon}$ and ω are computed from (3.3), (6.7) and the relation $\nu_1 = -\hat{\varepsilon}^2$ when α and γ are changed. Some numerical computations obtained by the computer software AUTO [12], in which the approaches are described in Appendix A, are also provided.

Figure 14 shows saddle-node bifurcation sets of harmonic orbits ($m, n = 1$) as well as heteroclinic bifurcation sets, detected by Propositions 6.1 and 6.2. In the regions between the two curves in Figs. 14(a) and (b), respectively, there exist transversely heteroclinic and harmonic orbits near the unperturbed heteroclinic

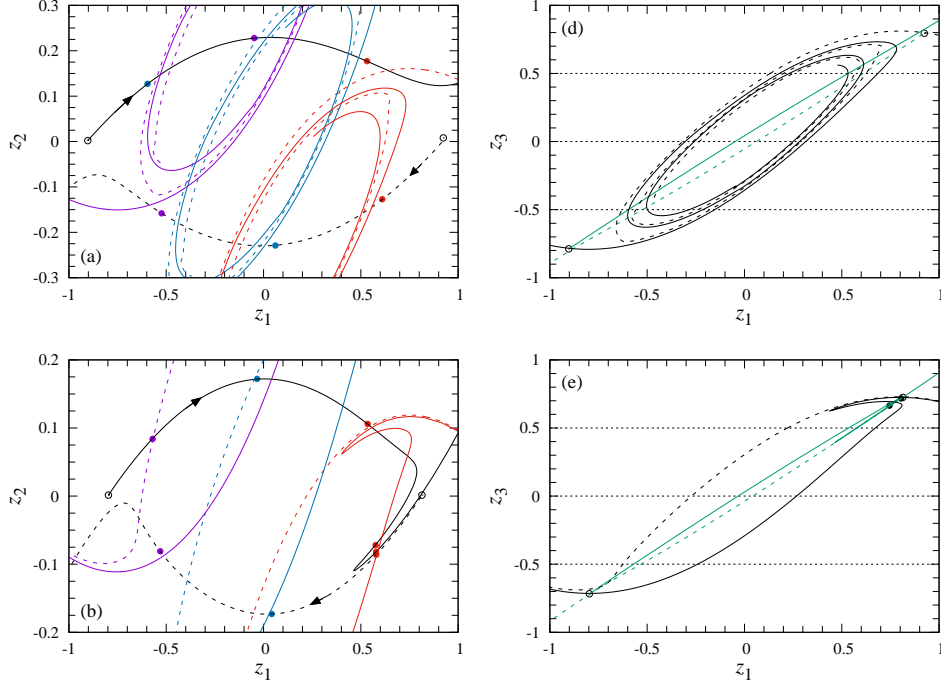


FIGURE 15. Stable and unstable manifolds of periodic orbits in (1.1) with (1.7) on the Poincaré section $\{t = 0 \pmod{2\pi/\omega}\}$ for $\alpha = 1.5$, $\theta_0 = 0$, $\delta_0 = 0.2$, $\delta_1 = -1.2$, $\beta = 5$ and $\hat{\omega} = 1.4$: (a) and (d) $\gamma = -1.1$; (b) and (e) $\gamma = -1.342915$; (c) and (f) $\gamma = -1.4$. The circle represents the periodic orbit. In Figs. (a)-(c), the black line represents the projection of the unstable manifold onto the (z_1, z_2) -plane, the small purple, blue and red disks, respectively, represent the intersections of the unstable manifold with the planes $z_3 = -0.5, 0$ and 0.5 , and the purple, blue and red lines, respectively, represent the intersections of the stable manifolds with the planes $z_3 = -0.5, 0$ and 0.5 onto the (z_1, z_2) -plane. In Figs. (d)-(f), the black lines represent the intersections of the stable manifold with the plane $z_2 = 0$, the green line represents the projection of the unstable manifold onto the (z_1, z_3) -plane, and the small black disks represent the intersections of the unstable manifold with the planes $z_2 = 0$. The solid and dashed lines represent these intersections or projections for the left and right periodic orbits, respectively.

and periodic orbits with $\varepsilon = 0$ (see Figs. 12(c) and 14(a) of [27]). In Fig. 14(b), numerical computations by AUTO are also plotted as broken lines and found to agree well with the theoretical prediction, especially near the codimension-two bifurcation point $(\alpha, \gamma) = (1, -1)$.

Figure 15 shows the numerically computed stable and unstable manifolds of periodic orbits near the unperturbed saddles with $\varepsilon = 0$, the behavior of which is described in Proposition 6.1, for $\alpha = 1.5$, $\hat{\omega} = 1.4$ and $\gamma = -1.1, -1.342915$

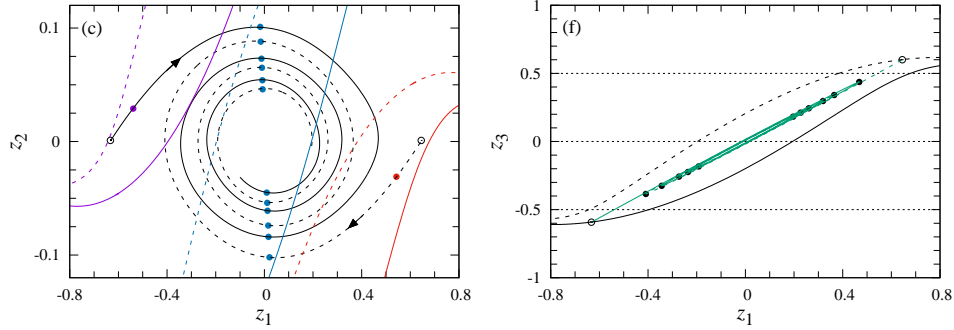


FIGURE 15. Continued.

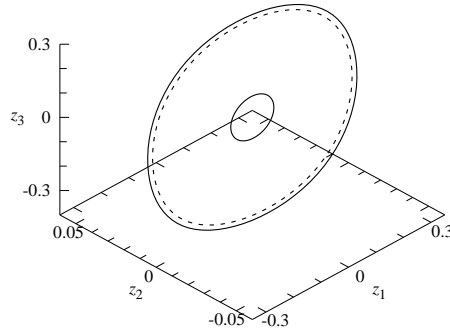


FIGURE 16. Harmonic orbits ($m, n = 1$) in (1.1) with (1.7) for $\alpha = 1.25$, $\gamma = -1.2$, $\theta_0 = 0$, $\delta_0 = 0.2$, $\delta_1 = -1.2$, $\beta = 5$ and $\hat{\omega} = 0.8$. The solid and broken lines, respectively, represent stable and unstable ones.

or -1.4 . It was numerically observed in Fig. 14(a) of [27] that there exist a pair of heteroclinic orbits in (1.1) with $\theta_d = 0$ (i.e., $\varepsilon = 0$) for $\gamma \approx -1.342915$. We see that these manifolds intersect transversely in Fig. 15(b) while they do not in Figs. 15(a) and (c). Their behavior in Figs. 15(a), (b) and (c) is, respectively, similar to plates ①, ③ and ⑤ of Fig. 6(c).

Figure 16 shows numerically computed periodic orbits of period $2\pi/\omega$ for $\alpha = 1.25$ and $\gamma = -1.2$. The two large ones are born at the saddle-node bifurcation detected by Proposition 6.2: One of them is stable and the other is unstable, as predicted there. The small one, which is continued from the equilibrium at the origin with ε from $\varepsilon = 0$, always exists near it when $\varepsilon > 0$ is sufficiently small.

The values of α, γ used in Figs. 14-16 are not necessarily close to the codimension-two bifurcation point $(\alpha, \gamma) = (1, -1)$ and they are rather far from it in some cases. Thus, our theoretical results are still valid even in such a situation although it does not satisfy our assumption in the theory.

6.3. Case of $\theta_0 = \pi$. We turn to the case of $\theta_0 = \pi$, in which $s_1, s_2 = -1$. We first assume that $\nu_1 < 0$. Let $\nu_1 = -\hat{\varepsilon}^2$ and define $\hat{\omega}, \Delta$ as in (3.3). We compute (3.15)

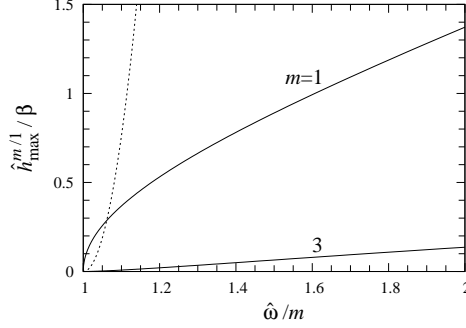


FIGURE 17. Dependence of $\hat{h}_{\max}^{m/1}$ on $\hat{\omega}$ for $\alpha_0 = 1$, $\gamma_0 = 1$, $\delta_0 = 0.5$ and $m = 1, 3$ in Proposition 6.3.

for (4.3) as

$$\begin{aligned} \hat{h}^{m/n}(\phi) &= -\frac{9\sqrt{3}k\beta\gamma_0\delta_0^3}{\alpha_0^{5/2}(\alpha_0 + \delta_0)^{9/2}(1 - 2k^2)} \\ &\quad \times \int_0^{m\hat{T}} \operatorname{sn}\left(\frac{t}{\sqrt{1-2k^2}}\right) \operatorname{dn}\left(\frac{t}{\sqrt{1-2k^2}}\right) \cos(\hat{\omega}t + \phi) dt \\ &= \begin{cases} \frac{18\sqrt{3}\pi\beta\gamma_0\delta_0^3\hat{\omega}}{\alpha_0^{5/2}(\alpha_0 + \delta_0)^{9/2}} \operatorname{sech}\left(\frac{m\pi K(k')}{2K(k)}\right) \sin\phi & \text{if } m \text{ is odd and } n = 1; \\ 0 & \text{otherwise,} \end{cases} \end{aligned}$$

where the resonance relation $nT^k = m\hat{T} = 2m\pi/\hat{\omega}$ has been used. Using Theorem 4.1 and Remark 4.2, we obtain the following.

Proposition 6.3. *Let $\theta_0 = \pi$ and let $m > 0$ be an odd integer. Then saddle-node bifurcations of $2m\pi/\omega$ -periodic orbits around $z = (\pi, 0, 0)$ occur in (1.1) with (1.7) near the two curves given by (3.17) with*

$$\hat{h}_{\max}^{m/1} = \frac{18\sqrt{3}\pi\beta\gamma_0\delta_0^3\hat{\omega}}{\alpha_0^{5/2}(\alpha_0 + \delta_0)^{9/2}} \operatorname{sech}\left(\frac{m\pi K(k')}{2K(k)}\right), \quad \hat{h}_{\min}^{m/1} = -\hat{h}_{\max}^{m/1}.$$

Moreover, one of the periodic orbits born at the bifurcations is of a sink or saddle type, depending on whether

$$\hat{h}_{\max}^{m/1}, \hat{h}_{\min}^{m/1} < \frac{1}{\Delta} \left(\frac{J_1(k, 1)J_3(k, 1)}{m\hat{T}} + J_2(k, 1) \right) \quad (6.9)$$

or the opposite of inequality holds while the other is always a saddle.

The dependence of $\hat{h}_{\max}^{m/1}$ on $\hat{\omega}$ when $\alpha_0 = 1$, $\gamma_0 = 1$ and $\delta_0 = 0.5$ is shown for $m = 1, 3$ in Fig. 17. The values of $\hat{h}_{\max}^{m/1}$ for $m \geq 5$ are very small compared with those for $m = 1, 3$. Condition (6.9) always holds for both \hat{h}_{\max} and \hat{h}_{\min} , i.e., one of the periodic orbits born at the saddle-node bifurcations given by the first and second equations of (3.17) is of a sink type.

We next assume that $\nu_1 > 0$. Let $\nu_1 = \hat{\varepsilon}^2$ and define $\hat{\omega}, \Delta$ as in (3.3). We compute (3.7) for (4.7) as

$$\begin{aligned}\hat{h}(\phi) &= \mp \frac{9\sqrt{3}\beta\gamma_0\delta_0^3}{\alpha_0^{5/2}(\alpha_0 + \delta_0)^{9/2}} \int_{-\infty}^{\infty} \operatorname{sech} t \tanh t \cos(\hat{\omega}t + \phi) dt \\ &= \pm \frac{9\sqrt{3}\pi\beta\gamma_0\delta_0^3\hat{\omega}}{\alpha_0^{5/2}(\alpha_0 + \delta_0)^{9/2}} \operatorname{sech}\left(\frac{\pi\hat{\omega}}{2}\right) \sin \phi,\end{aligned}$$

and (3.15) for (4.8) and (4.9) as

$$\begin{aligned}\hat{h}^{m/n}(\phi) &= \mp \frac{9\sqrt{3}k^2\beta\gamma_0\delta_0^3}{(\alpha_0(\alpha_0 + \delta_0))^{5/2}(2 - k^2)} \\ &\quad \times \int_0^{m\hat{T}} \operatorname{sn}\left(\frac{t}{\sqrt{2 - k^2}}\right) \operatorname{cn}\left(\frac{t}{\sqrt{2 - k^2}}\right) \cos(\hat{\omega}t + \phi) dt \\ &= \begin{cases} \pm \frac{9\sqrt{3}\pi\beta\gamma_0\delta_0^3\hat{\omega}}{\alpha_0^{5/2}(\alpha_0 + \delta_0)^{9/2}} \operatorname{sech}\left(\frac{m\pi K(k')}{K(k)}\right) \sin \phi & \text{if } n = 1; \\ 0 & \text{otherwise} \end{cases}\end{aligned}$$

and

$$\begin{aligned}\hat{h}^{m/n}(\phi) &= - \frac{9\sqrt{3}k\beta\gamma_0\delta_0^3}{\alpha_0^{5/2}(\alpha_0 + \delta_0)^{9/2}(2k^2 - 1)} \\ &\quad \times \int_0^{m\hat{T}} \operatorname{sn}\left(\frac{t}{\sqrt{2k^2 - 1}}\right) \operatorname{dn}\left(\frac{t}{\sqrt{2k^2 - 1}}\right) \cos(\hat{\omega}t + \phi) dt \\ &= \begin{cases} \frac{18\sqrt{3}\pi\beta\gamma_0\delta_0^3\hat{\omega}}{\alpha_0^{5/2}(\alpha_0 + \delta_0)^{9/2}} \operatorname{sech}\left(\frac{m\pi K(k')}{2K(k)}\right) \sin \phi & \text{if } m \text{ is odd and } n = 1; \\ 0 & \text{otherwise,} \end{cases}\end{aligned}$$

respectively, where the resonance relation $nT^k = m\hat{T} = 2m\pi/\hat{\omega}$ has been used. Using Theorems 4.3-4.5 and Remark 4.6, we obtain the following.

Proposition 6.4. *Let $\theta_0 = \pi$. There exist a periodic orbit near $z = (\pi, 0, 0)$ in (1.1) with (1.7) such that its stable and unstable manifolds intersect transversely in both sides if for $|\nu_1|, |\nu_2|, \varepsilon > 0$ sufficiently small condition (4.11) or equivalently (4.12) holds with*

$$\hat{h}_{\max} = \frac{9\sqrt{3}\pi\beta\gamma_0\delta_0^3\hat{\omega}}{\alpha_0^{5/2}(\alpha_0 + \delta_0)^{9/2}} \operatorname{sech}\left(\frac{\pi\hat{\omega}}{2}\right), \quad \hat{h}_{\min} = -\hat{h}_{\max}.$$

Moreover, homoclinic bifurcations occur near the two curves given by (4.13) or equivalently by (4.14).

Proposition 6.5. *Let $\theta_0 = \pi$ and let $m > 0$ be an integer. Then saddle-node bifurcations of $2m\pi/\omega$ -periodic orbits in both sides of $z = (\pi, 0, 0)$ occur in (1.1) with (1.7) near the two curves given by (4.15) or equivalently by (4.16) with*

$$\hat{h}_{\max}^{m/1} = \frac{9\sqrt{3}\pi m\beta\gamma_0\delta_0^3\hat{\omega}}{\alpha_0^{5/2}(\alpha_0 + \delta_0)^{9/2}} \operatorname{sech}\left(\frac{m\pi K(k')}{K(k)}\right), \quad \hat{h}_{\min}^{m/1} = -\hat{h}_{\max}^{m/1}.$$

Moreover, one of the periodic orbits born at the bifurcations is of a sink or saddle type, depending on whether

$$\begin{aligned} \hat{h}_{\max}^{m/1}, \hat{h}_{\min}^{m/1} &> -\frac{1}{\Delta} \left(\frac{J_1(k, 1)J_3(k, 1)}{m\hat{T}} - J_2(k, 1) \right) \\ \left(\text{resp. } \hat{h}_{\max}^{m/1}, \hat{h}_{\min}^{m/1} &< \frac{1}{\Delta} \left(\frac{J_1(k, 1)J_3(k, 1)}{m\hat{T}} - J_2(k, 1) \right) \right) \end{aligned} \quad (6.10)$$

or the opposite of inequality holds, while the other is always a saddle.

Proposition 6.6. *Let $\theta_0 = \pi$ and let $m > 0$ be an odd integer. Then saddle-node bifurcations of $2m\pi/\omega$ -periodic orbits encircling the pair of homoclinic orbits to $z = (\pi, 0, 0)$ for $\varepsilon = 0$ occur in (1.1) with (1.7) near the two curves given by (4.17) with*

$$\hat{h}_{\max}^{m/1} = \frac{18\sqrt{3}\pi m\beta\gamma_0\delta_0^3\hat{\omega}}{\alpha_0^{5/2}(\alpha_0 + \delta_0)^{9/2}} \operatorname{sech} \left(\frac{m\pi K(k')}{2K(k)} \right), \quad \hat{h}_{\min}^{m/1} = -\hat{h}_{\max}^{m/1}.$$

Moreover, one of the periodic orbits born at the bifurcations is of a sink or source type, depending on whether

$$\hat{h}_{\max}^{m/1}, \hat{h}_{\min}^{m/1} > -\frac{1}{\Delta} \left(\frac{J_1(k, 1)J_3(k, 1)}{m\hat{T}} - J_2(k, 1) \right) \quad (6.11)$$

or the opposite of inequality holds, while the other is always a saddle.

Figure 18(a) displays the dependence of \hat{h}_{\max} on $\hat{\omega}$ in Proposition 6.4, and Figs. 18(b) and (c) display the dependence of $\hat{h}_{\max}^{m/1}$ on $\hat{\omega}$ for $m = 1-6$ and $m = 1, 3, 5, 7, 9$, in Propositions 6.5 and 6.6, respectively, when $\alpha_0 = 1$, $\gamma_0 = 1$ and $\delta_0 = 0.5$. Condition (6.10) was shown numerically to always hold for \hat{h}_{\max} and \hat{h}_{\min} in Fig. 18(c), i.e., one of the periodic orbits born at the saddle-node bifurcations given by (4.15) or (4.16) is of a sink type, Condition (6.11) was also shown numerically to always hold in Fig. 18(c).

Henceforth we fix $\delta_0 = 0.5$, $\delta_1 = 0.5$, and $\Delta = 1$, so that $\alpha_0 = 1$ and $\gamma_0 = 1$. The values of ε , $\hat{\varepsilon}$ and ω are computed from (3.3), (6.7) and the relation $\nu_1 = -\hat{\varepsilon}^2$ or $\hat{\varepsilon}^2$ when α and γ are changed. Numerical computations obtained by the computer tool AUTO [12] are also given (see Appendix A for the approach used).

Figure 19 shows saddle-node bifurcation sets of harmonic orbits ($m, n = 1$) as well as homoclinic bifurcation sets, detected by Propositions 6.3-6.6. The saddle-node bifurcation sets in Figs. 19(a), (b) and (c) were plotted by using Propositions 6.3, 6.5 and 6.6, respectively. In the regions between the two curves there exist transversely homoclinic and harmonic orbits near the unperturbed homoclinic and periodic orbits with $\varepsilon = 0$ (see Figs. 13(b) and (d) and 14(b) of [27]). Numerical computations by AUTO for saddle-node bifurcation sets are also plotted as broken lines and found to agree well with the theoretical predictions, especially near the codimension-two bifurcation point $(\alpha, \gamma) = (1, 1)$. In some cases, the agreement between theoretical and numerical ones is almost complete.

Figure 20 shows the numerically computed stable and unstable manifolds of periodic orbits near the origin, the behavior of which are described in Proposition 6.4, for $\alpha = 0.8$, $\hat{\omega} = 1.4$ and $\gamma = 0.7, 0.7471888$ or 0.78 . It was numerically observed in Fig. 14(b) of [27] that there exist a pair of homoclinic orbits in (1.1) with $\theta_d = \pi$

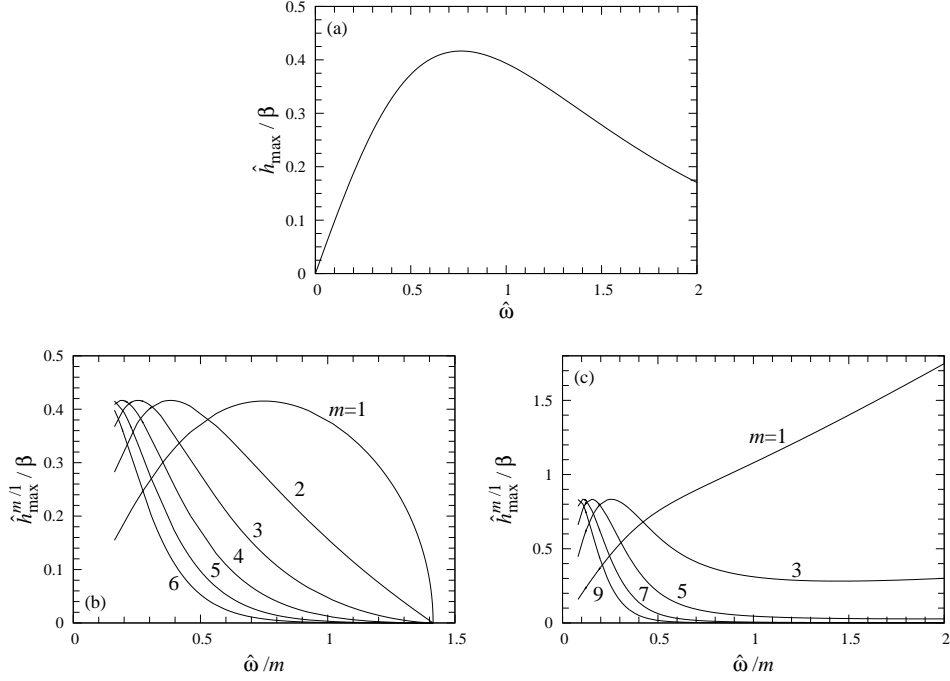


FIGURE 18. Dependence of \hat{h}_{\max} and $\hat{h}_{\max}^{m/1}$ on $\hat{\omega}$ for $\alpha_0 = 1, \gamma_0 = 1$ and $\delta_0 = 0.5$ in Propositions 6.4-6.6: (a) \hat{h}_{\max} ; (b) $\hat{h}_{\max}^{m/1}$ for $m = 1-6$ in Proposition 6.5; (c) $\hat{h}_{\max}^{m/1}$ for $m = 1, 3, 5, 7, 9$ in Proposition 6.6.

(i.e., $\varepsilon = 0$) for $\gamma \approx 0.7471888$. We observe that these manifolds intersect transversely in Fig. 20(b) while they do not in Figs. 20(a) and (c). Their behavior in Figs. 20(a), (b) and (c) are, respectively, similar to cases ①, ③ and ⑤ of Fig. 10(c).

Figure 21 shows numerically computed periodic orbits of period $2\pi/\omega$ for $\alpha = 1.25$ and $\gamma = -1.2$. Periodic orbits born at saddle-node bifurcations detected by Propositions 6.3, 6.5 and 6.6 are displayed in Figs. 21(a), (b) and (c), respectively, while small periodic orbits, which are continued from the equilibria at $z = (\pi, 0, 0)$ for $(\alpha, \gamma) = (1.2, 1.3)$ and given by (A.1) for $(\alpha, \gamma) = (0.8, 0.7)$ with ε from $\varepsilon = 0$ and always exist near them when $\varepsilon > 0$ is sufficiently small, are also plotted in Figs. 21(a) and (b). One of the periodic orbits bifurcated at the saddle-node bifurcations is stable and the other is unstable, as predicted by these propositions.

The values of α, γ used in Figs. 19-21 are not necessarily close to the codimension-two bifurcation point $(\alpha, \gamma) = (1, 1)$ and they are rather far from it in some cases. Thus, our theoretical results are still valid even in such a situation although it does not satisfy our assumption in the theory, as in Section 6.2.

ACKNOWLEDGMENTS

The author would like to thank Takeshi Inoue for his assistance. This work was partially supported by the JSPS KAKENHI Grant Number JP17H02859.

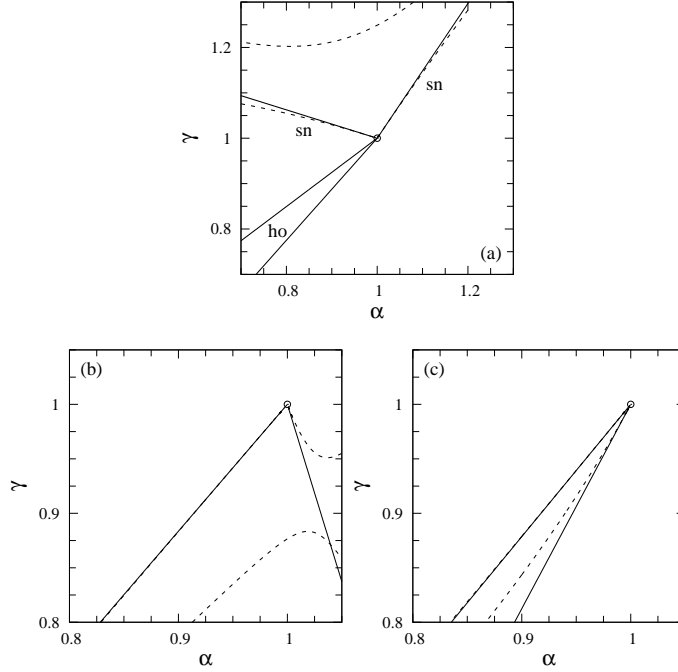


FIGURE 19. Bifurcation sets in (1.1) with (1.7) for $\theta_0 = \pi$, $\delta_0 = 0.5$, $\delta_1 = 0.5$ and $\beta = 5$: (a) Homoclinic and saddle-node bifurcations for $\hat{\omega} = 1.4$; (b) and (c) saddle-node bifurcations for $\hat{\omega} = 0.8$. The circle represents the codimension-two bifurcation point. The solid and broken lines, respectively, represent the theoretical predictions and numerical results for the saddle-node bifurcations. The labels “ho” and “sn”, respectively, represent heteroclinic and saddle-node bifurcations in Fig. (a). Bifurcations of periodic orbits inside and outside of the homoclinic orbits are plotted in Figs. (b) and (c).

APPENDIX A. NUMERICAL ANALYSES FOR (1.1) WITH (1.7)

In this appendix we describe our approach to obtain numerical results of Section 6 for (1.1) with (1.7) by the computer software AUTO [12]. The following two cases were considered:

- (i) $\theta_0 = 0$, $\delta_0 = 0.2$, $\delta_1 = -1.2$, $\beta = 5$ and $\hat{\omega} = 1.4$ or 0.8 ;
- (ii) $\theta_0 = \pi$, $\delta_0 = 0.5$, $\delta_1 = 0.5$, $\beta = 5$ and $\hat{\omega} = 1.4$ or 0.8 .

Several values of α and γ were taken, and the values of β and $\hat{\omega}$ were changed during some numerical continuations. We have $(\alpha_0, \gamma_0, \sigma) = (1, -1, 1)$ and $(1, 1, -1)$ in cases (i) and (ii), respectively. We also took $\Delta = 1$ in (3.3), so that

$$\omega = \hat{\varepsilon} \frac{\alpha_0(\alpha_0 + \delta_0)\hat{\omega}}{3\delta_0}, \quad \varepsilon = \hat{\varepsilon}^4, \quad \hat{\varepsilon} = \frac{3\delta_0 \sqrt{|\tilde{a}_{21}\alpha_1 + \tilde{b}_{21}\gamma_1|}}{\alpha_0(\alpha_0 + \delta_0)},$$

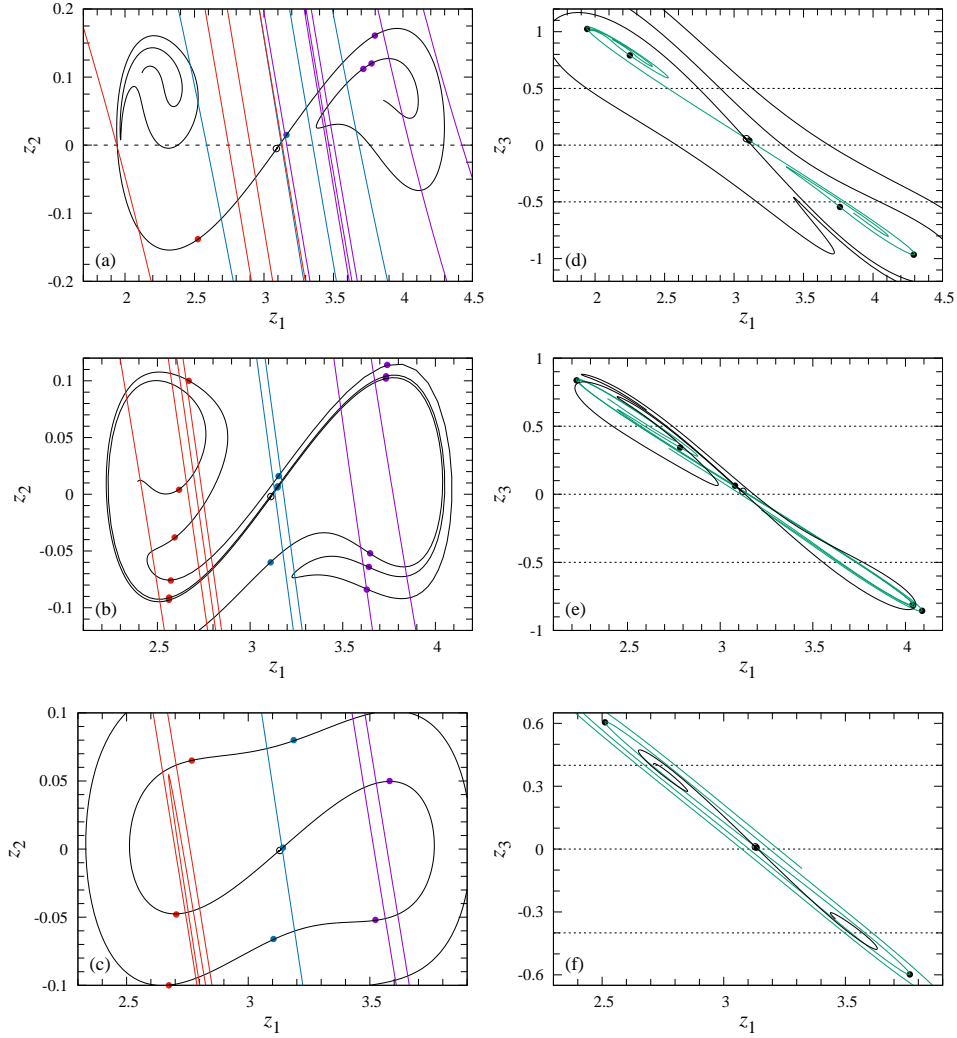


FIGURE 20. Stable and unstable manifolds of a periodic orbit in (1.1) with (1.7) on the Poincaré section $\{t = 0 \pmod{2\pi/\omega}\}$ for $\alpha = 0.8$, $\theta_0 = \pi$, $\delta_0 = 0.5$, $\delta_1 = 0.5$, $\beta = 5$ and $\hat{\omega} = 1.4$: (a) and (d) $\gamma = 0.7$; (b) and (e) $\gamma = 0.7471888$; (c) and (f) $\gamma = 0.78$. In Fig. (c), the small purple, blue and red disks, respectively, represent the intersections of the unstable manifold with the planes $z_3 = -0.4, 0$ and 0.4 , and the purple, blue and red lines, respectively, represent the intersections of the stable manifolds with the planes $z_3 = -0.4, 0$ and 0.4 onto the (z_1, z_2) -plane. See the caption of Fig. 15 for the meaning of the other lines and symbols and those in the other figures.

where $\alpha_1 = \alpha - \alpha_0$ and $\gamma_1 = \gamma - \gamma_0$. Numerical results of the codimension-two bifurcations with symmetry in (1.1) with $\theta_d = \theta_0$ (i.e., $\varepsilon = 0$ in (1.7)) for these parameter values are found in [27] (see Figs. 10 and 11 there especially).

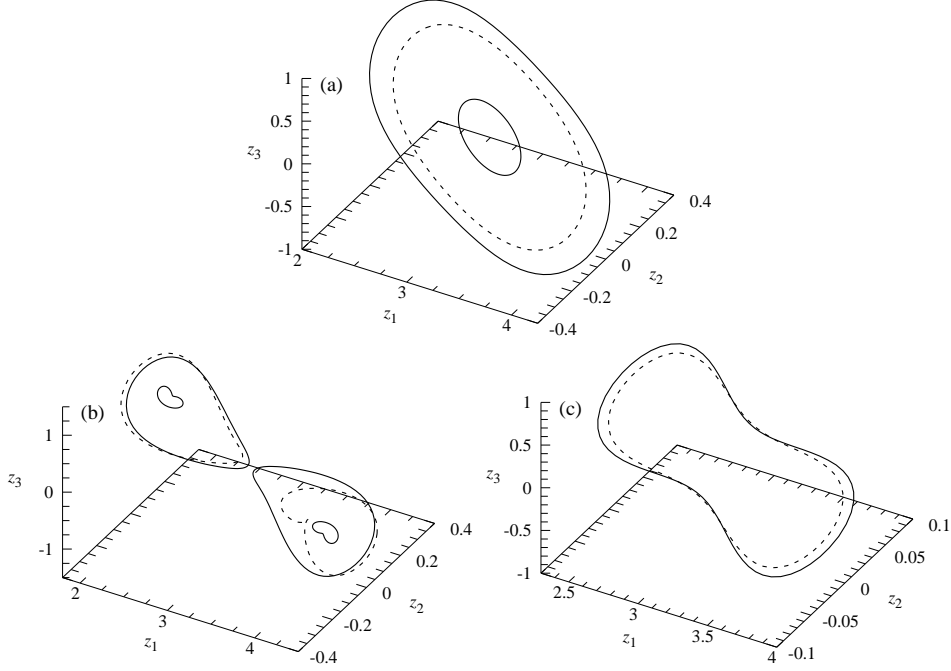


FIGURE 21. Periodic orbits in (1.1) with (1.7) for $\theta_0 = \pi$, $\delta_0 = 0.5$ and $\delta_1 = 0.5$: (a) $\alpha = 1.2$, $\gamma = 1.3$, $\beta = 5$ and $\hat{\omega} = 1.4$; (b) $\alpha = 0.8$, $\gamma = 0.7$, $\beta = 5$ and $\hat{\omega} = 0.8$; (c) $\alpha = 0.9$, $\gamma = 0.87$, $\beta = 5$ and $\hat{\omega} = 0.8$. The solid and broken lines, respectively, represent stable and unstable ones.

A.1. Bifurcations of periodic orbits. We took the following approach for numerical bifurcation analyses of periodic orbits by the computer tool AUTO except for periodic orbits encircling the unperturbed homoclinic orbits in case (ii), such as plotted in Fig. 21(c). The equilibrium

$$z = (4.024683666180083, 0, -0.7727046360165037) \\ \text{or } (2.258501640999503, 0, 0.7727046360165037) \quad (\text{A.1})$$

was chosen as the starting solution at $\beta = 0$ for $\gamma = 0.7$ in case (ii), or $z = (\theta_0, 0, 0)$ with $\theta_0 = 0$ or π for the other cases, and periodic orbits with a period of $2\pi/\omega$ were numerically continued from the equilibria when β was increased. After that, the periodic orbits with $\beta = 5$ were continued with γ , and saddle-node bifurcations were detected. The saddle-node bifurcations were continued with the two parameters α, γ , and the corresponding bifurcation sets in the (α, γ) -plane were obtained. Here the forcing term ' $\varepsilon\beta \cos \omega t$ ' was computed as a solution to a two-dimensional autonomous system as in the AUTO demo `frc` [12].

For periodic orbits encircling the unperturbed homoclinic orbits in case (ii), such an orbit at $\beta = 0$ was computed in advance by AUTO and chosen as the starting solution with $\omega = 2\pi/\tilde{T}$, where \tilde{T} is its period. The periodic orbit was numerically continued with ω , and the approach stated above was followed after that.

TABLE 1. A pair of saddles in (1.1) with $\theta_d = 0$ for $\alpha = 1.5$, $\delta_0 = 0.2$ and $\delta_1 = -1.2$. Here the upper or lower sign is taken simultaneously for each saddle and $z_2 = 0$.

γ	z_1	z_3
-1.3	± 0.9132926875617018	± 0.7915203292201416
-1.342915	± 0.8056567435744962	± 0.7212856838648964
-1.4	± 0.6389467723304353	± 0.5963503208417396

A.2. Computation of stable and unstable manifolds. As in [29], we reduce the computation of stable and unstable manifolds of periodic orbits to a boundary value problem of differential equations. See, e.g., Section 5.3 of [29] for more details.

From the numerical results of [27] (see Fig. 14 there especially) we see that there exist pairs of heteroclinic orbits and homoclinic orbits to equilibria for $(\alpha, \gamma) \approx (1.5, -1.342915)$ and $(0.8, 0.7471888)$ in cases (i) and (ii), respectively, when $\beta = 0$. Trajectories on the stable and unstable manifolds of the equilibria for $\beta = 0$ were computed in advance by AUTO with the assistance of the HomCont library [9, 10, 12]. Here the equilibria depend on the value of γ in case (i) while the equilibrium does not change at $z = (\pi, 0, 0)$ in case (ii). The loci of the equilibria in case (i) used for Fig. 15 are given in Table 1. The computed trajectories were chosen as the starting solutions and continued with β or their time length or endpoints. The saddle-type periodic orbits were also computed at the same time.

The reader may consider that we can numerically continue (transverse) homoclinic and heteroclinic orbits and compute homoclinic and heteroclinic bifurcation sets like the periodic orbits and saddle-node bifurcation sets in Appendix A.1. However, we did not succeed in it since the period of the saddle-type periodic orbits is very long and the moduli of related positive and negative eigenvalues are very small.

REFERENCES

- [1] V. I. Arnold, Lectures on bifurcations in versal families, *Russian Math. Surveys*, **27** (1972), 54–123.
- [2] V. I. Arnold, *Mathematical Method of Classical Mechanics*, 2nd ed., Springer, New York, 1989.
- [3] P.W. Bates, K. Lu and C. Zeng, Existence and persistence of invariant manifolds for semiflows in Banach space, *Mem. Amer. Math. Soc.*, **135** (1998), no. 645.
- [4] P.W. Bates, K. Lu and C. Zeng, Persistence of overflowing manifolds for semiflow, *Comm. Pure Appl. Math.*, **52** (1999), 983–1046.
- [5] H.W. Broer, R. Roussarie, and C. Simó, Invariant circles in the Bogdanov-Takens bifurcation for diffeomorphisms, *Ergodic Theory Dynam. Systems*, **16** (1996), 1147–1172.
- [6] K. Burns and H. Weiss, A geometric criterion for positive topological entropy, *Comm. Math. Phys.*, **172** (1995), 95–118.
- [7] P.F. Byrd and M.D. Friedman, *Handbook of Elliptic Integrals for Engineers and Physicists*, Springer, Berlin, 1954.
- [8] J. Carr, *Applications of Centre Manifold Theory*, Springer, New York, 1981.
- [9] A.R. Champneys and Y.A. Kuznetsov, Numerical detection and continuation of codimension-two homoclinic bifurcation analysis, *Int. J. Bifurcation Chaos*, **5** (1996), 867–887.
- [10] A.R. Champneys, Y.A. Kuznetsov and B. Sandstede, A numerical toolbox for homoclinic bifurcations, *Int. J. Bifurcation Chaos*, **4** (1994), 795–822.
- [11] S.-N. Chow, C. Li and D. Wang, *Normal Forms and Bifurcation of Planar Vector Fields*, Cambridge Univ. Press, Cambridge, 1994.

- [12] E. Doedel and B.E. Oldeman, *AUTO-07P: Continuation and Bifurcation Software for Ordinary Differential Equations*, 2012, available online from <http://cmvl.cs.concordia.ca/auto>.
- [13] J. Eldering, *Normally Hyperbolic Invariant Manifolds: The Noncompact Case*, Atlantis Press, Paris, 2013. Springer
- [14] N. Fenichel, Persistence and smoothness of invariant manifolds for flows, *Indiana Univ. Math. J.*, **21** (1971), 193–225.
- [15] N. Fenichel, Asymptotic stability with rate conditions, *Indiana Univ. Math. J.*, **23** (1974), 1109–1137.
- [16] J. Guckenheimer and P. Holmes, *Nonlinear Oscillations, Dynamical Systems, and Bifurcations of Vector Fields*, Springer, New York, 1983.
- [17] M. Haragus and G. Iooss, *Local Bifurcations, Center Manifolds, and Normal Forms in Infinite-Dimensional Dynamical Systems*, Springer, London, 2011.
- [18] Y.A. Kuznetsov, *Elements of Applied Bifurcation Theory*, 3rd ed., Springer, New York, 2004.
- [19] J.A. Sanders, F. Verhulst and J. Murdock, *Averaging Methods in Nonlinear Dynamical Systems*, Springer, New York, 2007.
- [20] F. Takens, Singularities of vector fields, *Inst. Hautes Études Sci. Publ. Math.*, **43** (1974), 47–100.
- [21] S. Wiggins, *Normally Hyperbolic Invariant Manifolds in Dynamical Systems*, Springer, New York, 1994.
- [22] S. Wiggins, *Introduction to Applied Nonlinear Dynamical Systems and Chaos*, 2nd ed., Springer, New York, 2003.
- [23] K. Yagasaki, Chaos in a pendulum with feedback control, *Nonlinear Dynam.*, **6** (1994), 125–142.
- [24] K. Yagasaki, The Melnikov theory for subharmonics and their bifurcations in forced oscillations, *SIAM J. Appl. Math.*, **56** (1996), 1720–1765.
- [25] K. Yagasaki, Second-order averaging and Melnikov analyses for forced non-linear oscillators, *J. Sound Vib.*, **190** (1996), 587–609.
- [26] K. Yagasaki, A simple feedback control system: bifurcations of periodic orbits and chaos, *Nonlinear Dynam.*, **9** (1996), 391–417.
- [27] K. Yagasaki, Codimension-two bifurcations in a pendulum with feedback control, *Int. J. Non-Linear Mech.*, **34** (1999), 983–1002.
- [28] K. Yagasaki, Melnikov’s method and codimension-two bifurcations in forced oscillations, *J. Differential Equations*, **185** (2002), 1–24.
- [29] K. Yagasaki, Heteroclinic transition motions in periodic perturbations of conservative systems with an application to forced rigid body dynamics, *Regul. Chaotic Dyn.*, **23** (2018), 438–457.

DEPARTMENT OF APPLIED MATHEMATICS AND PHYSICS, GRADUATE SCHOOL OF INFORMATICS,
KYOTO UNIVERSITY, YOSHIDA-HONMACHI, SAKYO-KU, KYOTO 606-8501, JAPAN

Email address: yagasaki@amp.i.kyoto-u.ac.jp